Learning Cardiac Imaging

100 Essential Cases

Bearbeitet von
Ramón Ribes, Paola Kuschnir, Antonio Luna, Joan C Vilanova, José Manuel Jimenez-Hoyuela

1. Auflage 2009. Taschenbuch. xiv, 151 S. Paperback
ISBN 978 3 540 79082 2
Format (B x L): 19,3 x 26 cm

Echocardiography 2

Paola Kuschnir
Gustavo Avegliano, Marcelo Trivi, and Ricardo Ronderos (Contributors)

Introduction

From its first steps in the diagnosis of cardiovascular diseases, echocardiography imaging, such as M-mode, 2-D echocardiography and cardiovascular Doppler, has made tremendous advances until today. From primitive equipment that encouraged creativity and imagination, to 3-D echo, which shows structures the way surgeons see them during cardiac surgery, it has been an unthinkable journey for the pioneers in echocardiography.

Nowadays, echocardiography is the most widely used imaging technique for the diagnosis of cardiovascular diseases. This expansion was the result of a number of advantages such as its non-invasive low-risk nature, easy transportation of equipment, simplicity, and low cost. Moreover, there has been considerable improvement in image quality as a result of the development of transesophageal echocardiography and the technological advance of transthoracic transducers.

Echocardiography has contributed to the understanding and description of several cardiovascular diseases. Some paradigmatic examples are valvular diseases and hypertrophic and restrictive cardiomyopathies. Also the non-compaction of the left ventricular myocardium and Tako Tsubo syndrome are “echo diseases”. The concept of mechanical dyssynchrony is mainly echocardiographic.

The Achilles’ heel of echocardiography is that it is an explorer-dependent technique, which demands in-depth knowledge, the use of a well-defined methodology, and sound clinical correlation.

This chapter aims to show a series of pathologies that are seen in high-volume services, in order to enlighten those who have similar cases. All have been selected following a thorough learning approach and assessment protocols. We looked for cases where the diagnosis left no doubts.

Our goal is to show both the benefits of transthoracic and transesophageal echocardiography for different cardiovascular diseases and the usefulness of the wide range of available tools: 2D echo, conventional and tissue Doppler, contrast echo, 3D echo, etc. We also show further capabilities of the technique in the monitoring of invasive surgical and percutaneous procedures.

Finally, we focus on the relevance of echocardiography for the interpretation of patophysiological processes, clinical decision-making and prognosis.

Case 2.1
Apical Myocardial Hypertrophy

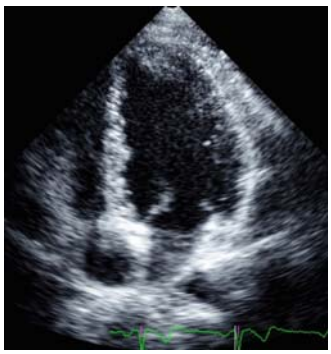

Fig. 2.1.1

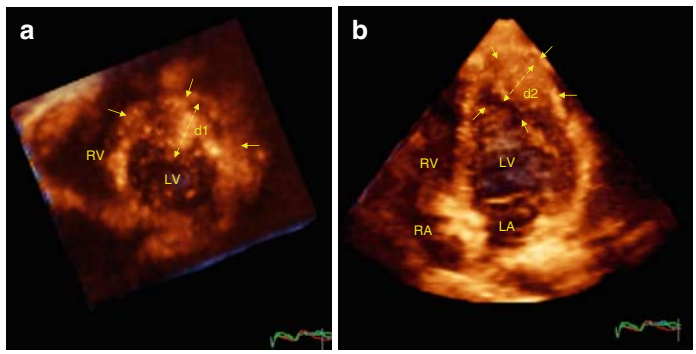

Fig. 2.1.2

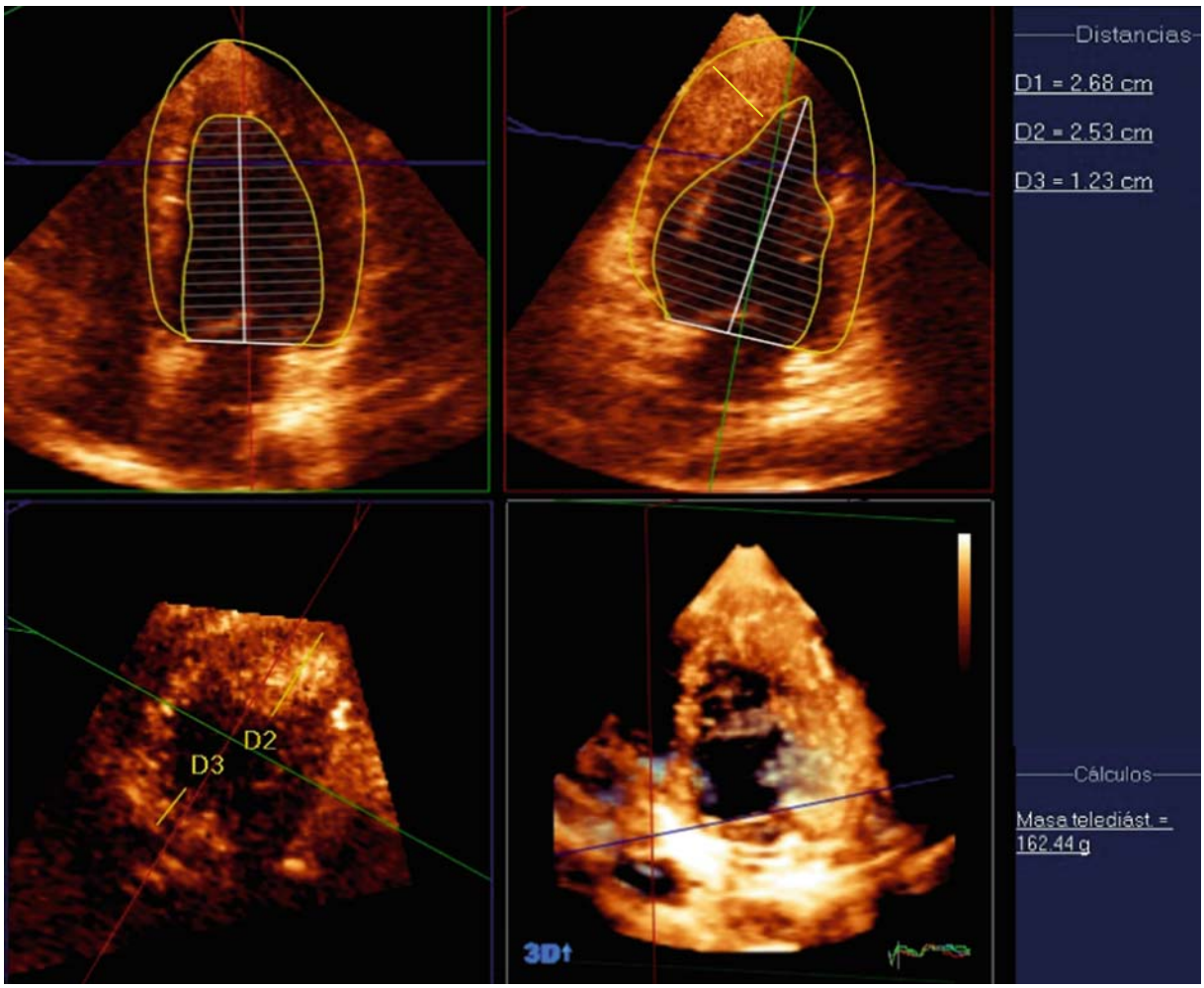

Fig. 2.1.3

A 29-year-old man with prior history of smoking presented to the emergency department complaining of oppressive chest pain. An electrocardiogram (ECG) showed asymmetric negative T waves in leads I, aV_L, V_2 to V_4. Cardiac enzymes were normal. The patient underwent noninvasive nuclear imagining that ruled out cardiac ischemia. Transthoracic bidimensional (2DE) and real-time 3D imaging (RT3DE) echocardiogram were performed.

Comments

Apical hypertrophic cardiomyopathy (HCM) is characterized by localized hypertrophy at the apical left ventricular segments. A pathognomonic feature of apical HCM is the presence of deep symmetric T-wave inversion in the anterior precordial leads. The presence of these latter ECG changes frequently suggests its diagnosis in the asymptomatic form of the disease. Symptomatic patients present with typical (16%) or atypical (14%) angina, palpitations (10%), dyspnea on exertion (6%), or syncopal episodes (6%). This form of HCM usually has a benign course and a good long-term prognosis. Nevertheless, its overt ECG changes mandate clinical rule-out of severe epicardial coronary stenosis by noninvasive imaging.

Cardiac magnetic resonance imaging (MRI) is currently the most sensitive and specific available technique for the diagnosis of apical HCM. MRI has an excellent accuracy for the measurement of myocardial thickness, providing an adequate assessment of the degree and extension of myocardial hypertrophy. Still, due to cost constraints, routine screening usually starts with 2DE with harmonic imaging. As a second step, further evaluation with either contrast 2DE or MRI should be followed, especially in cases with high clinical suspicion or poor echo window.

RT3DE enables precise heart slicing through the apex. The latter is particularly difficult to perform with 2D echocardiography due to foreshortening. Furthermore, utilization of RT3DE allows acquisition of any given slice across the left ventricle, thus obtaining a better morphological characterization of the HCM (i.e., myocardial thickness and distribution) than standard 2DE.

Findings

Figure 2.1.1 2DE shows a nondiagnostic image at the apex.

Figure 2.1.2 Left ventricular volume imaging is obtained by RT3DE. (a) Note the presence of segmental myocardial hypertrophy at the apical level. RT3DE apical view, which shows maximal myocardial thickness at the anterior and lateral apical segments (*arrows*), d2 = 26 mm. (b) Four-chamber view eliminating the inferior heart region. Note the disproportional hypertrophy at the apical segment of the lateral wall (*arrows*), d1 = 27 mm.

Figure 2.1.3 RT3DE. Multiplanar image shows an asymmetric distribution of hypertrophy. Note the measurement of myocardial thickness and quantification of the left ventricular mass.

Case 2.2

Severe Mitral Insufficiency Secondary to Papillary Muscle Rupture

A 74-year-old woman with a history of arterial hypertension and essential thrombocythemia presented to the emergency room complaining of intermittent chest pain and severe dyspnea for 5 days. On arrival, the patient had bilateral pulmonary edema in addition to III/VI systolic murmur that radiated to the axilla suggestive of mitral regurgitation. ECG revealed mild ST-segment elevation in leads DII and aV_F. Lab results showed high platelet count (960,000/ml) and mild troponine I elevation (1.95 ng/ml). The patient underwent cardiac catheterization that showed only a mild lesion (20%) on the mid-portion of the arterial circumflex coronary artery. A Doppler echocardiogram was performed to further elucidate the etiology of this left-sided heart failure.

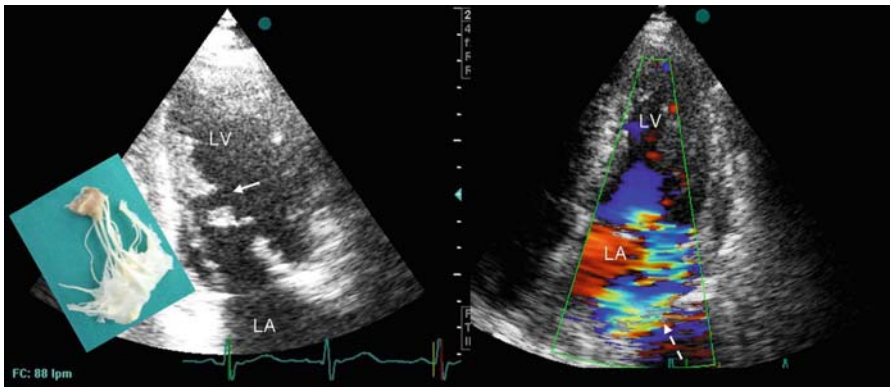

Fig. 2.2.1

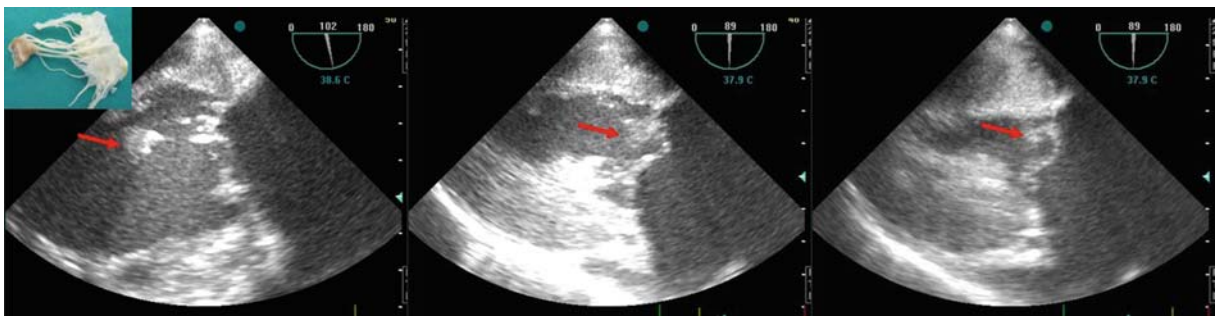

Fig. 2.2.2

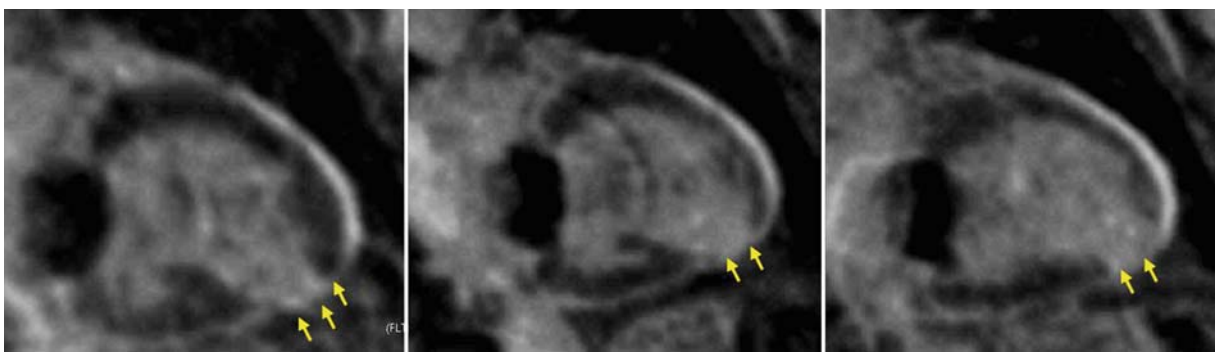

Fig. 2.2.3

Comments

Ischemic mitral regurgitation (MR) is due to either myocardial ischemia or infarction in the absence of primary structural valve abnormality. Moderate to severe ischemic MR during the acute phase of myocardial infarction is associated with a poor short- and long-term clinical outcome.

Ischemic MR is classified according to its presentation and pathophysiology: type I and II are due to acute ischemic injury linked to papillary muscle dysfunction (type I) or rupture (type II). Type III is related to fibrosis or sclerosis of the papillary muscle, likely due to an old myocardial infarction. Type IV is due to loss of the normal left ventricular architecture following a large myocardial infarction. Type III and IV have a more insidious presentation following an acute myocardial infarction than type I and II have.

An accurate understanding of the culprit mechanism of MR is of utmost importance in order to provide the best therapy for each individual case. Thus, type I ischemic MR may only require myocardial revascularization, while type II will definitely undergo either surgical mitral valve repair or replacement.

Transthoracic echocardiography (TTE) is very useful for the diagnosis and quantification of ischemic MR as well as the evaluation of the mechanism responsible for the disease. Furthermore, it enables an estimate of pulmonary arterial pressure and quantification of left ventricular systolic function. In our experience, mitral valve evaluation requires further imaging with transesophageal echocardiography (TEE), since its higher spatial resolution provides detailed information regarding the valve and its apparatus. In summary, we studied a peculiar case of acute myocardial infarction with nonsevere coronary stenosis at the time of catheterization complicated with posterior papillary rupture and severe acute MR.

Findings

Figure 2.2.1 *Left:* 2D TTE two-chamber view. In this image posterior papillary muscle rupture is clearly demonstrated (*continuous arrow*). Anatomic correlation of papillary muscle rupture is observed. In this particular case, both papillary muscles provide cords to both mitral leaflets. Note cusp rupture of the anterior leaflet, which presents abnormal closure. In the right image, color Doppler (four-chamber view) imaging reveals the presence of a mitral regurgitation jet (*dotted arrow*) coursing laterally to the left atrial wall.

Figure 2.2.2 Transgastric 90° TEE view. *Left*: image recorded at diastole showing the flail cusp of the posterior papillary muscle inside the left ventricle. *Center*: image at mid-systole showing posterior cusp folding to the ventricular side of the mitral valve. *Right*: image at late systole showing complete folding of the cusp and a striking prolapse of the anterior leaflet responsible for the presence of mitral valve insufficiency. Red arrows show the cusp of the papillary muscle.

Figure 2.2.3 Two-chamber DE-MRI view performed after surgical valve replacement, revealing transmural hyperintensity localized at the level of the mid- and apical segments of the inferior wall (*arrows*) with partial involvement of the posterior papillary muscle. Note artifact generated by the mitral valve prosthesis.

Case 2.3

Noncompacted Cardiomyopathy

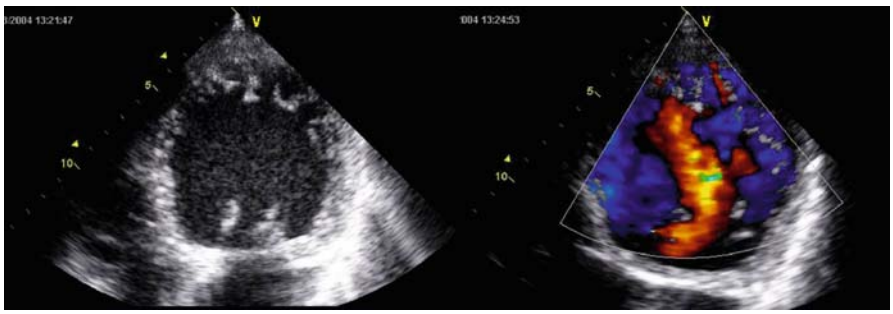

Fig. 2.3.1

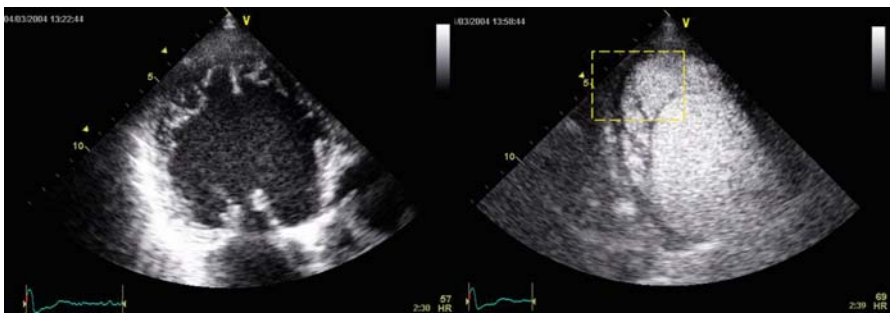

Fig. 2.3.2

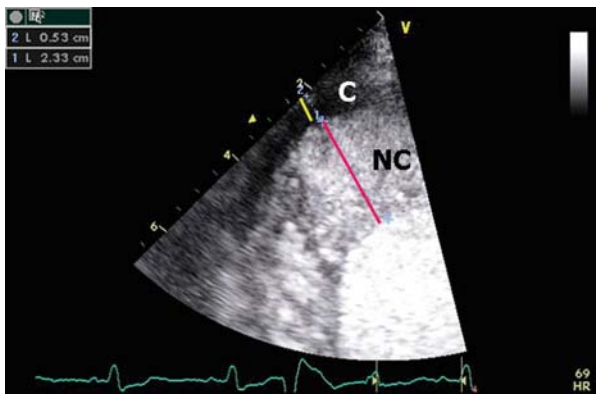

Fig. 2.3.3

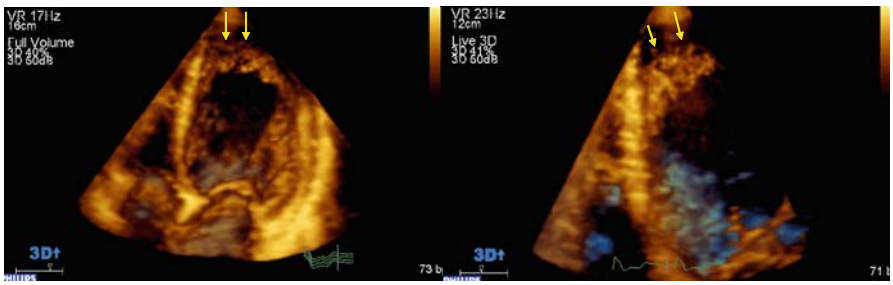

Fig. 2.3.4

A 37-year-old man, with no coronary risk factors, presented to our office complaining of palpitations and dyspnea on minimal exertion. An ECG demonstrated complete left bundle branch block. A chest X-ray showed cardiomegaly without any signs of venocapilar hypertension. Contrast and Doppler echocardiograms were performed to elucidate patient's cardiac condition.

Comments

Noncompaction cardiomyopathy (NCCM) is a recently characterized cardiomyopathy in which ventricular myocardial compactation fails to occur during fetal development. In NCCM, multiple large trabecules plus intertrabecular recesses are observed deep in the myocardium, especially at the apical segments. Imaging diagnostic criteria for NCCM require an area of noncompacted/compacted myocardium >2.3.

Various imaging techniques provide adequate sensitivity for the diagnosis of NCCM, and there are some cases when combining different techniques may be complementary. Bidimensional transthoracic echocardiography (2DE) is adequate for quantification of noncompacted myocardial regions, while visualization of compacted regions is cumbersome. Quantification of compacted myocardium with 2DE is greatly improved with the use of contrast agents. The author believes that contrast echocardiographic assessment of noncompacted/compacted myocardial index is best performed with zoom during diastole in regions where papillary muscles will not overlap (i.e., apical, latero-apical, and inferior-lateral).

Additional data can be obtained regarding the distribution and localization of noncompacted myocardial areas with RT3DE. Currently, MRI, due to its excellent spatial and tissue resolution, represents the most detailed and precise imaging technique for the assessment of NCCM. In addition, MRI is particularly useful in patients with mild form of the disease or in patients with poor echo window. Multidetector computed tomography of the heart also conveys myocardial morphological information, and can thus be an option especially in patients with suspected coronary artery disease. In summary, all the above-mentioned imaging techniques provide reliable data regarding the degree of trabeculation in the left ventricle. Nonetheless, NCCM diagnosis should not be performed with only one isolated measurement. Imaging data derived from morphological myocardial quantification and the assessment of global left ventricular function often need correlation with the patient's clinical condition and, in some cases, familial evaluation (i.e., genetic testing) in order to obtain an accurate diagnosis.

Findings

Figure 2.3.1 *Left*: 2DE, apical four-chamber view revealing large trabecules and deep intertrabecular recesses in the left ventricle. *Right*: Color flow Doppler signal filling these recesses.

Figure 2.3.2 *Left*: 2DE, apical three-chamber view demonstrates multiple deep trabecule formation inside the myocardium, which clearly defines the noncompacted myocardium. *Right*: The compacted area is visualized with contrast agent administration. The *square* (zoom) demarcates the studied myocardial region.

Figure 2.3.3 Contrast echo (with zoom) performed during diastole. Note how the compacted myocardium acquires a dark color, improving its visualization. The noncompacted/compacted myocardial index was greater than 2.5.

Fig 2.3.4 Left ventricular volume imaging is obtained by RT3DE. Showing the non compaction at the apical segments with RT3DE. *Left*: Four-chamber view eliminating the inferior heart region. Note the apical hipertrabeculation (*arrows*). *Right*: the same image with zoom.

Case 2.4
Right Atrial Tumor

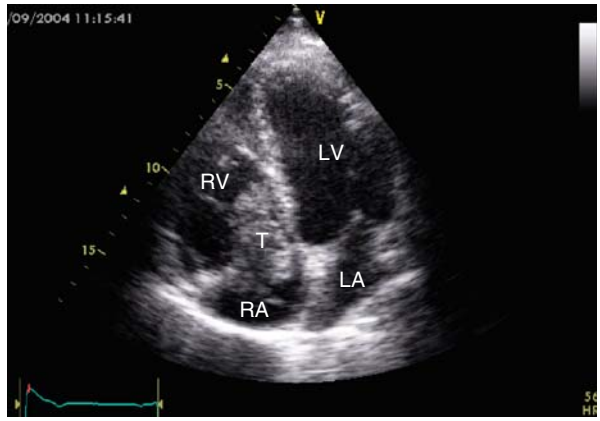

Fig. 2.4.1

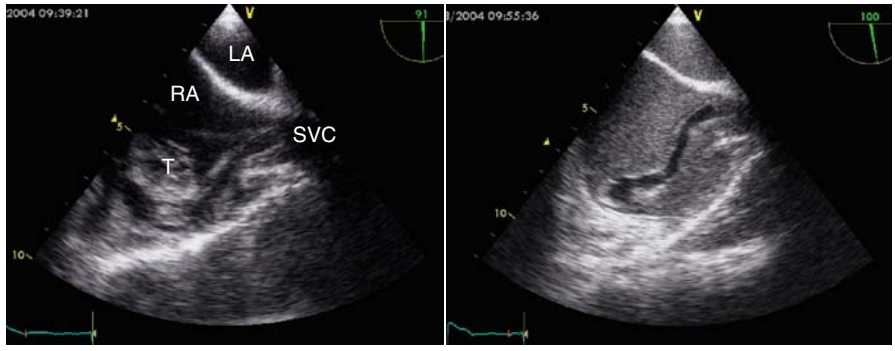

Fig. 2.4.2

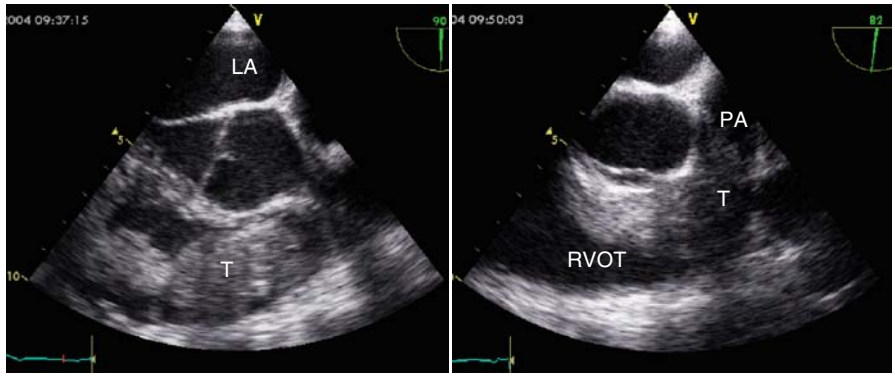

Fig. 2.4.3

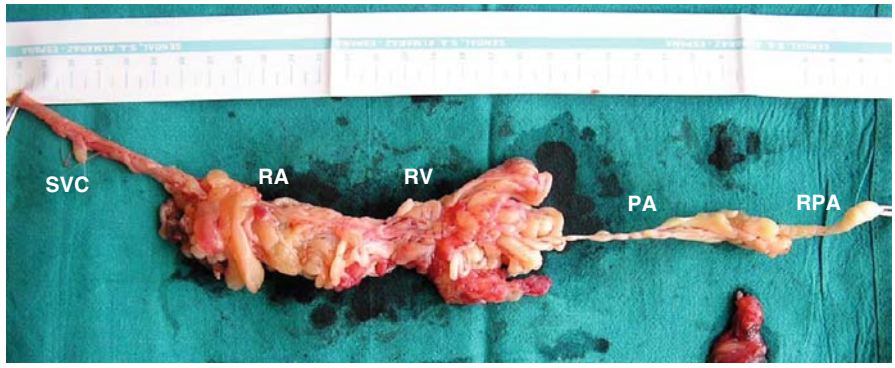

Fig. 2.4.4

A 38-year-old man with a prior history of testicular cancer presented to the emergency room with worsening dyspnea. One year prior to admission, he was diagnosed with metastatic non-seminomatous germ-cell tumor involving the lungs, the mediastinum, and the retroperitoneum. The patient underwent right orchiectomy and chemotherapy followed by surgical metastatic tissue resection, and remained asymptomatic until 1 week prior to this admission when he started feeling short of breath. Lung scan was performed and it revealed pulmonary embolisms in the mid and inferior right lobes. Then an echocardiogram was performed.

Comments

Primary cardiac tumors are infrequent. Benign mixomas account for half of all primary tumors. On the other hand, metastatic tumor involvement of the heart is much more common than primary cardiac tumors. In autopsy reports of patients with disseminated neoplasm, metastasis to the heart was found in 10–20% of the cases. Malignant melanoma most often involves the heart, followed by germ-cell tumors [e.g., metastasis to the heart was found in 38% of the necropsies performed in 100 patients with germ-cell tumors]. Transthoracic (TTE) and transesophageal (TEE) echocardiography are very instrumental in the morphological evaluation of cardiac masses and continues to be the first imaging techniques to be used in the presence of cardiac signs or symptoms potentially related to cardiac masses. TTE is readily available and offers sufficient spatial resolution plus adequate real-time imaging at low cost. Furthermore, its use provides clinically relevant information regarding valve function and the degree of hemodynamic compromise. Therefore, TTE represents the first imaging diagnostic step when dealing with cardiac masses. TEE enables a more detailed assessment of the size, mobility, and anchoring area of the tumor as well as its level of infiltration in cardiac structures. Magnetic resonance imaging (MRI) offers further details regarding tissue characterization and degree of infiltration of the tumor (e.g., pericardium and adjacent structures). Still, pathological confirmation is mandatory in all patients presenting with cardiac masses. This particular case shows a patient with right atrial tumor, found to be metastasis of a non-seminomatous germ-cell tumor.

Findings

Figure 2.4.1 TTE. Apical four-chamber view revealing a large mass with irregular borders through the tricuspid valve. *RV* right ventricle; *RA* right atrium; *T* tumor; *LV* left ventricle; *LA* left atrium.

Figure 2.4.2 TEE at the level of cavas. *Left*: Note a large tumoral mass that involves the superior vena cava as a low echogenic pedunculated mass, which is also observed in the right atrium as a multilobulated mass. *Right*: Contrast TEE unveils the vascular pedicle of the tumor (i.e., the contrast agent diffuses into the vascular region of the tumor and clearly delineates the peduncular area).

Figure 2.4.3 TEE. *Left*: 90° image revealing a mass that passes through the right ventricular outflow tract. *Right* image: the mass reaches the pulmonary artery trunk. *RVOT* right ventricular outflow tract; *PA* pulmonary artery trunk.

Figure 2.4.4 Macroscopic image of a surgically excised mass. Note the exact position of each portion of the mixoma within the heart and adjacent vascular structures. *SVC* superior vena cava; *RA* right atrium; *RV* right ventricle; *PA* pulmonary artery (trunk); *RPA* right pulmonary artery.

Case 2.5

Lateral Left Ventricular Wall Rupture Following Acute Myocardial Infarction

A 79-year-old man with a history of chronic obstructive pulmonary disease due to smoking and a long-standing history of coronary artery disease requiring surgical myocardial revascularization (left internal mammary artery to left anterior descending coronary artery and a vein graft to right coronary artery) 10 years prior to this admission presented with new onset of resting chest pain. ECG was normal. Cardiac catheterization showed patency of both grafts, left anterior descending coronary artery with proximal total occlusion, first diagonal with an 80% stenosis and first marginal of circumflex with a 90% stenosis. The patient underwent stenting of both diagonal and marginal lesions and remained asymptomatic for 76 h when he had a syncopal episode associated with severe bradicardia with fast recovery followed by complaints of chest pain. ECG showed diffuse ST-segment elevation. After 10 min, symptoms abated and ECG changes resolved. A diagnostic echocardiogram was performed.

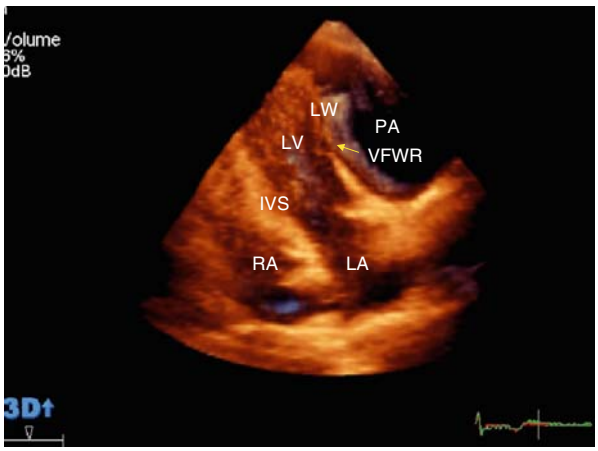

Fig. 2.5.3

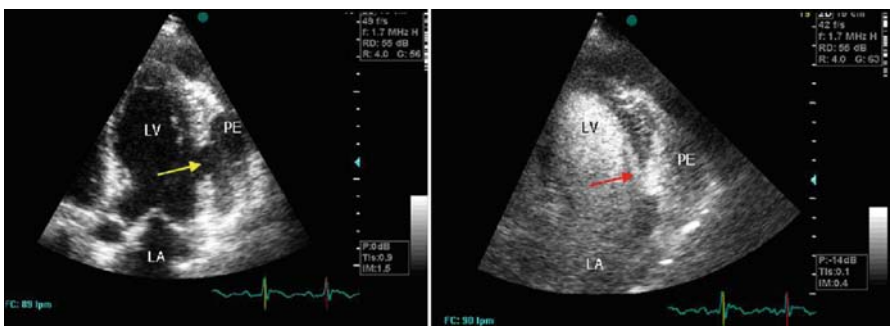

Fig. 2.5.1

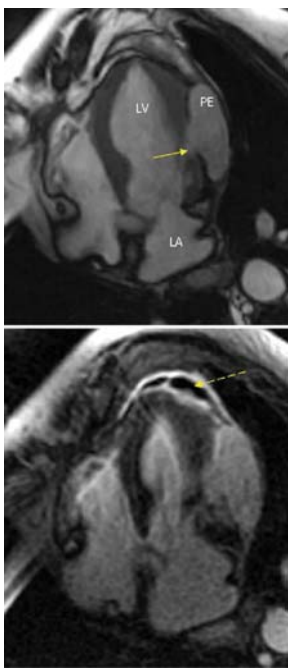

Fig. 2.5.2

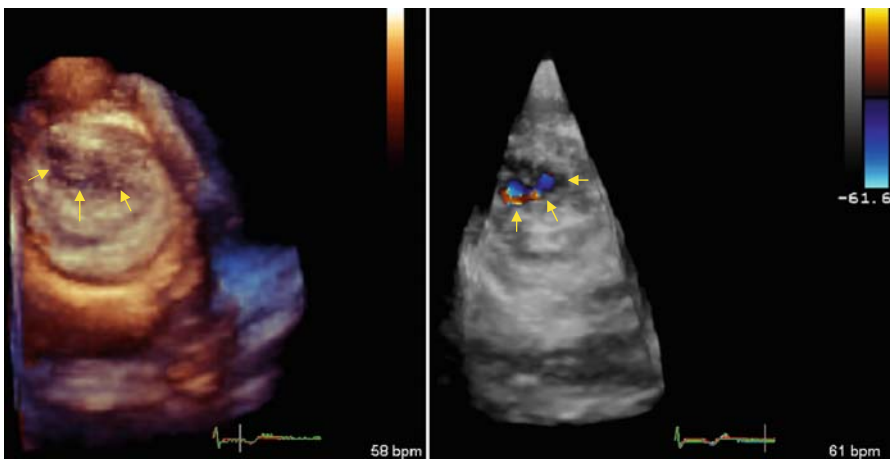

Fig. 2.5.4

Comments

Lateral left ventricular wall rupture (LWR) is a rare complication following acute myocardial infarction (AMI; 3–5%), reaching 10–25% in autopsy of AMI patients. After cardiogenic shock, LWR constitutes the most common cause of in-hospital death in AMI patients. Around 40% of all LWR occur during the first 24 h and 85% within the first week. It is frequently associated with advanced age, female gender, systemic arterial hypertension, absence of preinfarction angina, and no visible collaterals during catheterization. Diagnosis is suspected in patients with severe hypotension, extreme bradicardia, or cardiac arrest with electrical mechanical dissociation. Rupture is confirmed with echocardiographic evidence of a large pericardial effusion, with echoes suggestive of hemopericardium. As in the present case, patients with prior history of cardiac surgery may experience self-limited myocardial rupture with prompt sealing due to pericardial adhesions, resulting in a pseudoaneurysm. The development of a pseudoaneurysm after an AMI is exceedingly low and its natural evolution is unknown.

Usually, bidimensional and contrast TTE suffices for purposes of clinical diagnosis. On the other hand, real-time 3D echocardiography (RT3DE) gives greater anatomical and functional information than TTE and emerges as an exceptional imaging tool prior to surgical intervention. In the present case, 76 h following the intervention, LWR was observed likely due to a small infarction at the lateral left ventricular wall possibly because of the marginal lesion. Our patient refused surgery and was followed up clinically. Eighteen months later, RT3DE showed a consolidated pseudoaneurysm.

Findings

Figure 2.5.1 TTE (acute phase). *Left*: Note the rupture at the mid-portion of the lateral left ventricular wall (*arrow*) and a localized pericardial effusion adjacent to the lateral wall. *Right*: Contrast TTE. Note contrast filling of the pericardium and opacification of a parallel cavity, in relation to the left ventricle, with systolic and diastolic flow through the rupture.

Figure 2.5.2 MRI. *Left*: Cine-MRI (SSFP) at four-chamber view. Note the LWR (*arrow*) and localized pericardial effusion. *Right*: Delayed enhancement-MRI (inversion-recovery) following gadolinium administration. Presence of thrombotic pericardial adhesions in the apical region (*dashed arrow*). Absence of late enhancement (related to the complete loss of tissue compatible with a small transmural myocardial infarction). *LV* left ventricle; *LA* left atrium; *PE* pericardial effusion.

Figure 2.5.3 RT3DE performed at 18 months from the event. Full ventricular volume image revealing a consolidated pseudoaneurysm and the rupture area at the mid-portion of the left lateral ventricular wall (*arrow*). LV left ventricle; LA left atrium; RA right atrium; IVS interventricular septum; LW lateral wall; PA pseudoaneurysm; VFWR ventricular free wall rupture.

Figure 2.5.4 Three-dimensional echocardiogram. *Left*: Full 3D volume processed image. View of the lateral wall from the pseudoaneurysm (the *darkest area* demarcated by the *arrows* indicates the rupture area). *Right*: With color flow Doppler during diastole, note three *small points* suggesting regurgitant flow from the pseudoaneurysm to the left ventricular wall.

Case 2.6

Traumatic Rupture of the Tricuspid Valve

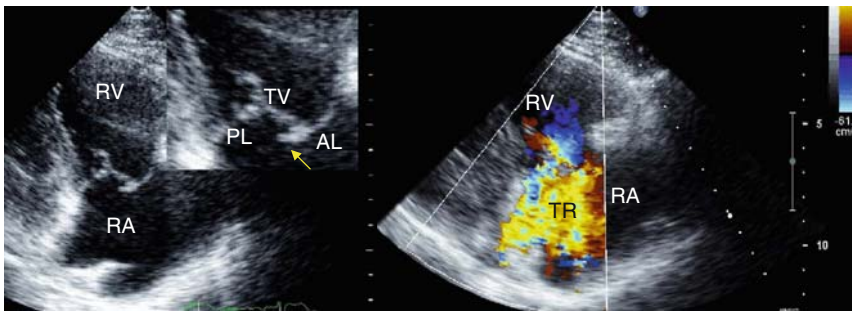

Fig. 2.6.1

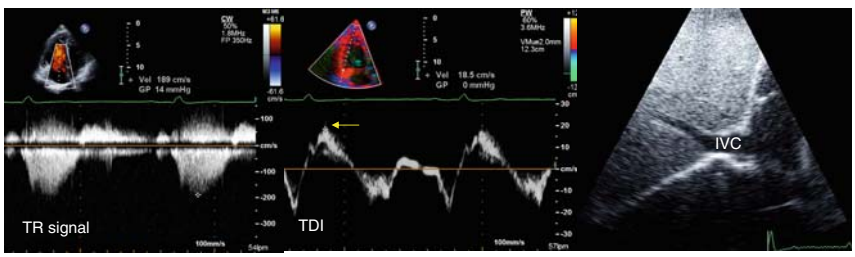

Fig. 2.6.2

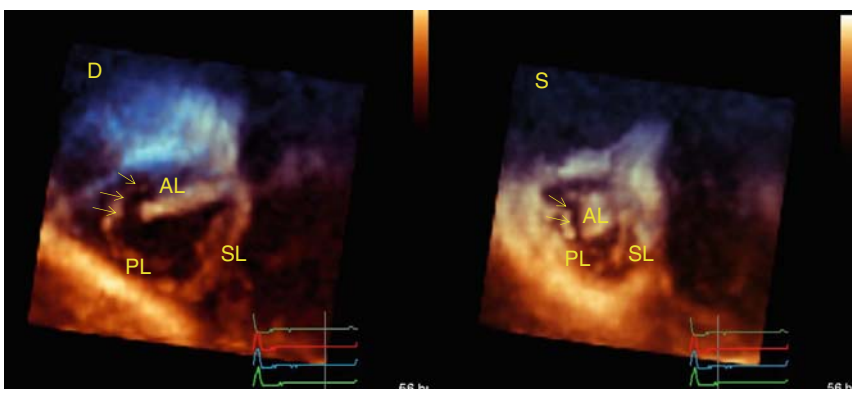

Fig. 2.6.3

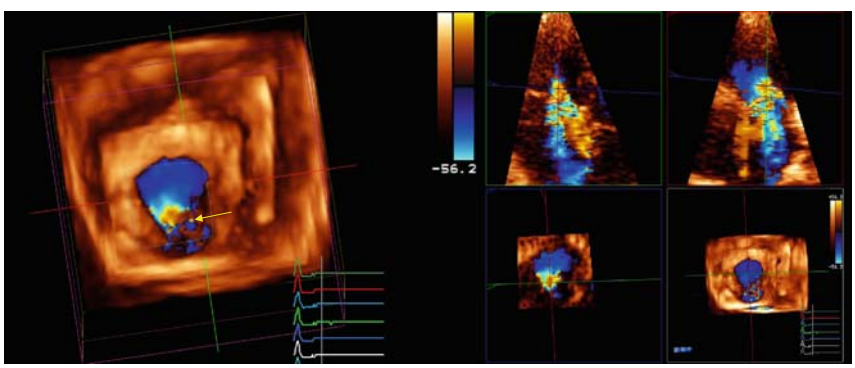

Fig. 2.6.4

A 39-year-old asymptomatic man is referred for an echocardiogram due to the presence of cardiac systolic murmur. He has no prior significant medical history, except for a motor vehicle accident (MVA) 3 years earlier.

Comments

MVA accounts for most cases of traumatic rupture of the tricuspid valve. Valve rupture during an MVA is generated by an abrupt deceleration coupled with an increase in right-side cardiac pressures (Valsalva maneuver and thorax compression). The most frequent rupture site is the tendinous cords, followed by the anterior papillary muscle and tear or detachment of the anterior leaflet. During the acute phase of an MVA, life-threatening lesions to the head, thorax, or abdomen are of most clinical relevance. Thus, accurate cardiac diagnosis during MVA is cumbersome, especially when dealing with discrete or moderate valve lesions. Diagnosis of tricuspid valve rupture is usually delayed, due to its mild clinical course. Echocardiography plays an important role in the diagnosis, follow-up, and surgical indication in patients with tricuspid valve rupture. Knowledge of right ventricle diameter and function in addition to data regarding the systemic venous circulation is of interest prior to tricuspid valve surgery. Performing color and tissue Doppler echocardiography plus cardiac magnetic resonance imaging represents the best combination prior to surgery. Finally, real-time 3D echocardiography (RT3DE) emerges as a novel useful imaging tool, offering a detailed anatomic and functional assessment of the tricuspid valve – useful data that may assess valve repair feasibility and decide the most appropriate repair technique.

Findings

Figure 2.6.1 TTE. *Left*: longitudinal view of the right ventricle during systole. Note the lineal image at mid-portion of the tricuspid anterior leaflet (*arrow*) compatible with cord rupture. Nevertheless, it is interesting how central coaptation is not lost. *Right side*: color Doppler image showing severe tricuspid regurgitation. *RA* right atrium; *RV* right ventricle; *PV* posterior valve; *AV* anterior valve; *TR* tricuspid regurgitation.

Figure 2.6.2 *From left to right*. Note the curve of tricuspid insufficiency without evidence of pulmonary arterial hypertension. RV function by tissue Doppler imaging was normal with a tricuspid annular systolic velocity >12 cm/seg (*arrow*), and inferior vena cava with normal inspiratory collapse suggests normal right-side cardiac and venous pressures despite volume overload.

Figure 2.6.3 RT3DE: Postprocessed full volume image. Tricuspid valve is viewed from the RV. *Left*: (diastole) Note a tear at the body of the anterior leaflet (*arrow*) and not at the chord, as suggested by bidimensional echo. The tear is observed from the free border to the annulus. *Right*: (systole) tricuspid valve is closed and folded. Note the persistence of lineal image indicative of anterior leaflet rupture (*arrow*).

Figure 2.6.4 RT3DE. *Left*: full volume color Doppler of the tricuspid valve from the RV, showing a regurgitant orifice through the rupture (*arrow*). *Right*: 3D multiplanar quantification of the three-dimensional regurgitant orifice, vena contracta, and hemisphere.

Case 2.7
Complicated Type B Aortic Dissection

A 61-year-old man with history of hypertension was admitted with acute aortic dissection type B. During his stay in the CCU, he complained of post-pandrial abdominal pain. Transesophageal echocardiogram (TEE) demonstrated compression of both celiac trunk

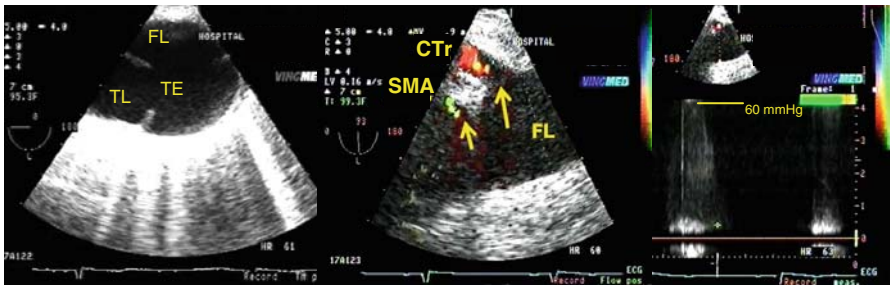

Fig. 2.7.1

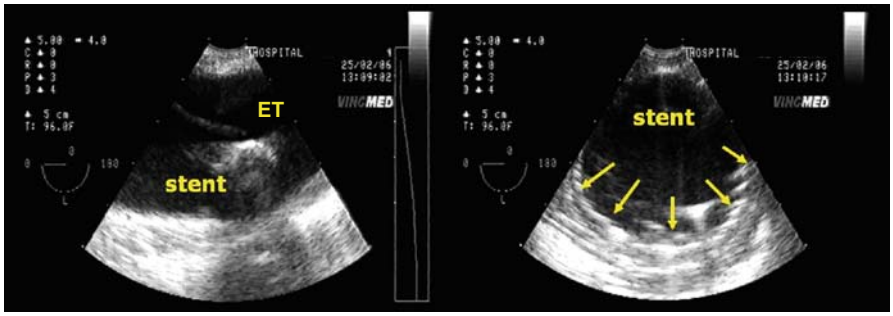

Fig. 2.7.2

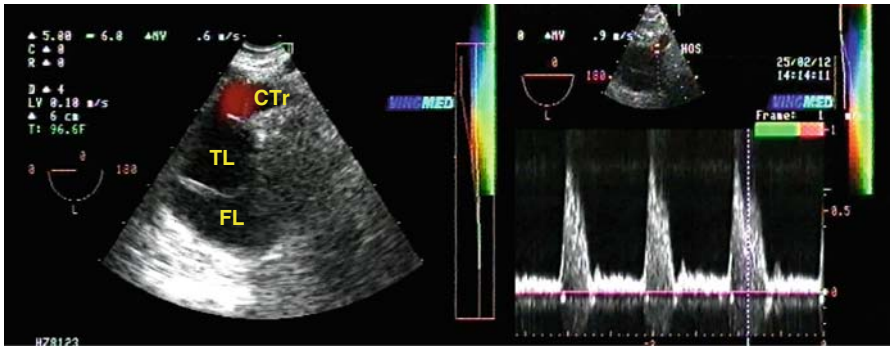

Fig. 2.7.3

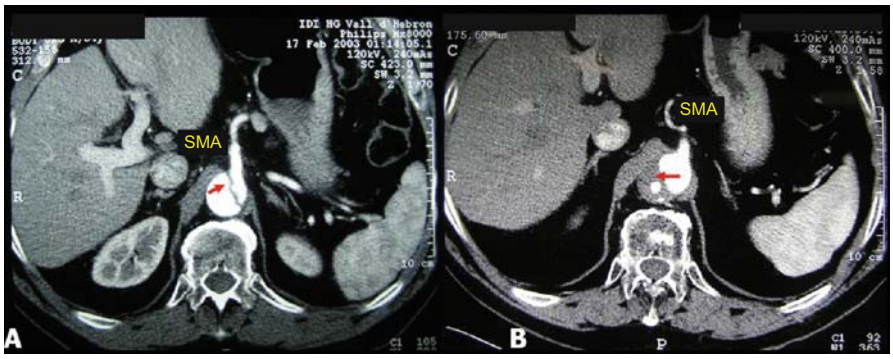

Fig. 2.7.4

(CTr) and superior mesenteric artery (SMA). Due to the presence of mesenteric ischemia as a complication of a type B aortic dissection, we proceeded with endovascular closure of the entry tear guided by imaging techniques with good results.

Comments

Acute aortic dissection (AAD) is the most frequent form of acute aortic syndromes and is also associated with the worst clinical outcome. Its mortality surpasses 60% during the first week if adequate treatment is not instituted fast. Besides cardiac complications, intimal dissection process can obstruct the ostium of several aortic arterial branches, with great potential for ischemia in a number of organs. Organ ischemia distally from the aortic dissection is frequently observed (30%). In the international registry of aortic dissection (IRAD), mesenteric ischemia was detected in 5.4% of the cases and it was associated with a high mortality risk. Early treatment of complicated dissections is crucial for patients' clinical course and long-term prognosis. Therefore, early and accurate diagnosis of arterial branch obstruction is needed in order to select the best therapeutic approach.

During an acute aortic syndrome, TEE allows rapid evaluation (≤15 min), at the patient's bedside or at the operating room, enabling an adequate monitoring of the patient's hemodynamics. TEE diagnostic sensitivity and specificity for the detection of aortic dissection is similar to other imaging techniques, providing location, size, and flow of the entry tear in addition to the degree of aortic insufficiency or presence of pericardial effusion/tamponade. In comparison with other imaging techniques, aortic arterial branch visualization by TEE is difficult, especially in the abdominal aorta. However, in centers with significant expertise accurate assessment of all abdominal aortic branches with TEE is feasible and provides complementary information to that obtained by computed tomography.

Findings

Figure 2.7.1 TEE. *Left*: transversal 0° view at the level of the proximal portion of the descending aorta proximally, where a large entry tear is observed. *Center*: longitudinal 93° view at the level of the CTr and SMA. Note the compression of both aortic branches secondary to intimal displacement due to elevated pressure at the false lumen (FL). In this image, the FL covers almost the entire aortic lumen and turbulence is clearly observed at the ostium of both aortic abdominal branches (*arrow*). *Right*: continuous Doppler signal at the level of the ostium of CTr demonstrating a 65 mmHg translational gradient compatible with severe obstruction. ET: entry tear, FL: false lumen, TL: true lumen, CTr: celiac trunck, SMA, superior mesenteric artery.

Figure 2.7.2 TEE monitoring during percutanous closure of the entry tear (ET). *Right*: 0° view of the aortic arch distally at the level of the entry tear showing correct placement of the stent prior to deployment. *Left*: similar image following stent deployment showing adequate stent apposition (*arrows*).

Figure 2.7.3 Quantification of CTr and SMA decompression. *Left*: transversal 0° view at the level of CTr, showing both patent branches with normal flow. *Right*: pulsed Doppler revealing normalization of systolic velocities with no significant gradient at the level of CTr and SMA (*arrows*).

Figure 2.7.4 *Left*: image taken prior to stent deployment showing compression of the SMA by the FL (*arrow*). *Right*: control image following EP closure. Note aortic and partial thrombosis of FL (*arrow*).

Case 2.8

Aortic Mobile Thrombosis

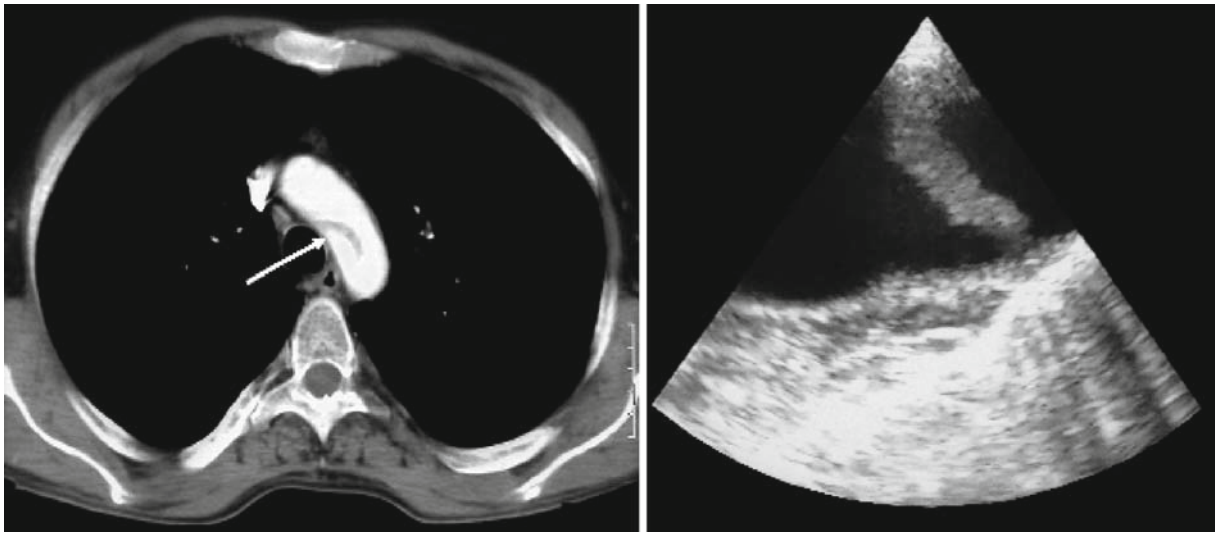

Fig. 2.8.1

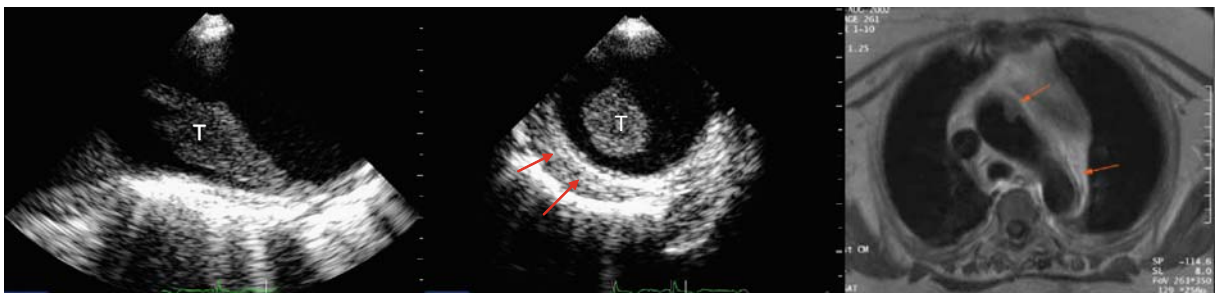

Fig. 2.8.2

We study two men who experienced acute limb ischemia. The first case is a 50-year-old patient with a history of dyslipidemia and new onset of upper left extremity ischemia, in which a computed tomography (CT) of the thorax was interpreted as aortic dissection at the arch level. The second case is an 80-year-old patient with low left extremity ischemia due to an embolic event in the clinical scenario of inflammation. Both cases underwent transesophageal echocardiogram (TEE).

Comments

Acute peripheral arterial ischemia may be the first manifestation of acute aortic dissection.

The presence of mobile aortic thrombosis is quite rare and is usually related to either complicated (i.e., ulcerated or debris accumulation) aortic plaques or to aortic aneurysms. Although rare, patients with nondilated otherwise normal aortas may develop an isolated aortic thrombus. In addition, the presence of aortic vasculitis can be unmasked by the detection of an aortic thrombus. Aortic thrombosis, particularly when the thrombus is mobile, is frequently associated with peripheral arterial embolism and may be mistaken for aortic dissection by some imaging techniques. Correct diagnosis is crucial because management differs in both entities.

As shown in the first case, TEE allows morphological characterization of the aortic wall and thrombus and rules out aortic dissection. The patient was started on antiplatelet and anticoagulant medications and thrombus regressed after 3 months. In the second case, mobile aortic thrombosis was in the context of vasculitis. The patient was diagnosed with giant cell arteritis (confirmed by temporal artery biopsy). The use of magnetic resonance imaging (MRI) in the second case was instrumental, showing inflammatory areas on the aortic wall, which helped obtain an accurate diagnosis.

Findings

Figure 2.8.1 (Case 1); *Right*: CT shows a linear image in the aortic arch (*arrow*) misdiagnosed as aortic dissection. Thrombus formation was interpreted as thrombosed intimal flap. *Left*: TEE reveals a 30-mm-long pedunculated thrombus in the aortic arch (patient 1).

Figure 2.82 (Case 2); TEE. *Left* and *center*: note a large pedunculated image with low echogenicity indicative of aortic thrombosis. The aortic vasculitic region presented thickening of the media layer and overt separation between adventitia and intima layers (*arrows*). *Right*: contrast MRI revealed a hyperintense signal suggestive of acute aortic inflammatory changes.

Case 2.9

Severe Mitral Insufficiency Secondary to Rupture of Posterior Leaflet

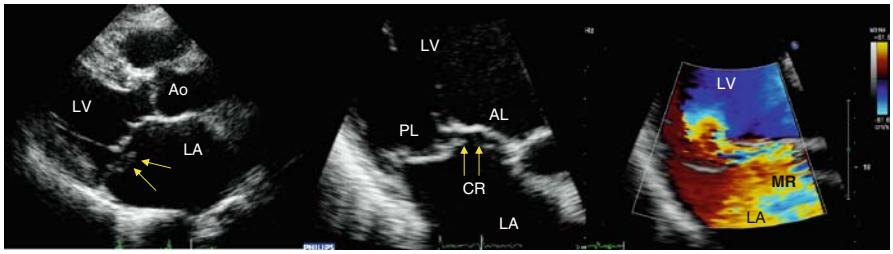

Fig. 2.9.1

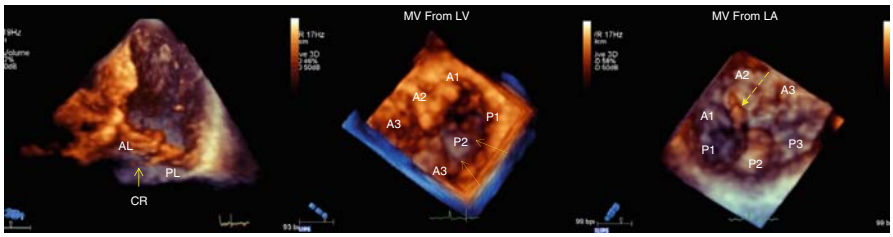

Fig. 2.9.2

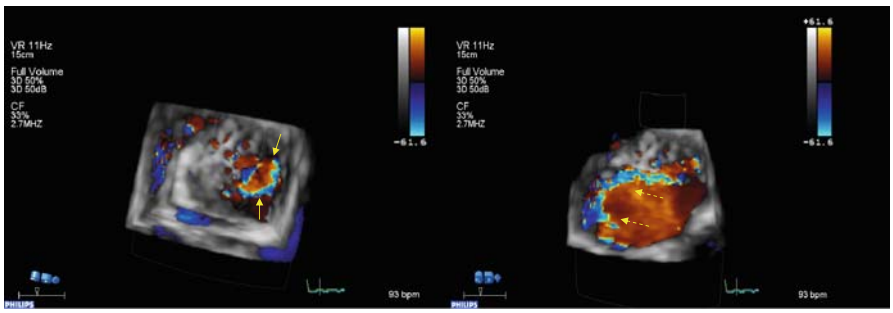

Fig. 2.9.3

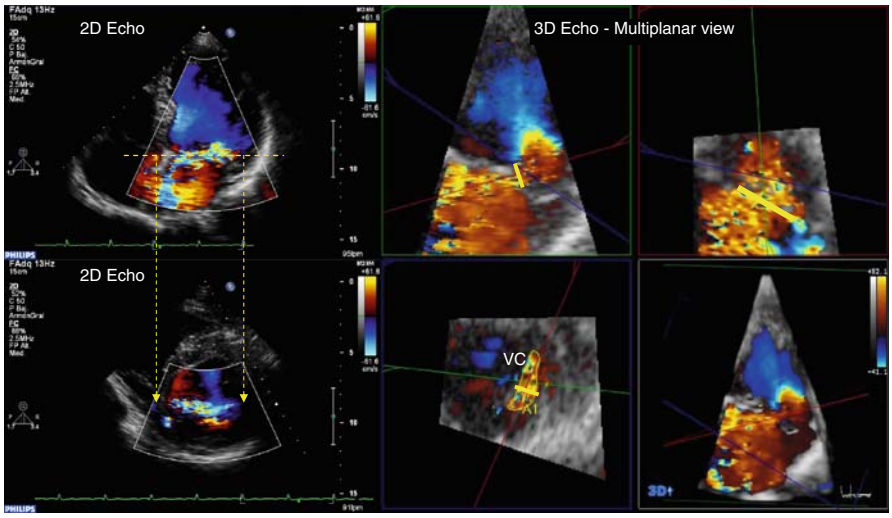

Fig. 2.9.4

A 52-year-old man, with no coronary risk factors, presented to our office complaining of dyspnea on exertion and palpitations. A systolic murmur was detected on auscultation and the patient underwent echocardiogram evaluation.

Comments

Mitral valve prolapse (MVP) has been described as the most common cardiac valvular abnormality in developed countries and the leading cause of mitral valve surgery for isolated mitral regurgitation (MR). Bidimensional echocardiography (2DE) is the most utilized imaging tool for diagnosing mitral valve disease, especially mitral valve prolapse. Occasionally, chordae tendinae of either the anterior or posterior mitral valve leaflet or both spontaneously rupture. Early detection and close surveillance of flail mitral valve is paramount due to its rapid progression to severe MR. Mitral valve repair is expected to provide better outcome than valve replacement, and requires a thorough understanding of mitral valve morphology. Echocardiographic evaluation is vital in order to determine the best timing for valve surgery. Conventional and color Doppler 2DE represents the first diagnostic tool for the diagnosis, quantification, and follow-up of flail mitral valve disease. In surgical candidates, transesophageal echocardiography (TEE) improves visualization of the valve and its apparatus, providing valuable data to gauge mitral valve repair feasibility and to evaluate surgical results. The emergence of real-time 3D echocardiography (RT3DE), either transthoracic or TEE, allows 3D reconstruction of the entire valve and its apparatus, which is a major improvement when compared to bidimensional images. RT3DE offers a great deal of morphological and functional information that helps understand different pathological mechanisms and plan an appropriate surgical strategy.

Findings

Figure 2.9.1 TTE 2DE. *Left*: paraesternal longitudinal view showing prolapse and eversion of the posterior leaflet (*arrows*). *Center*: three-chamber apical view with zoom. Note eversion of the posterior leaflet with rupture of the chordae (*arrows*). *Right*: three-chamber apical view with color Doppler image showing the origin of the regurgitant jet at the rupture site. *LV* left ventricle; *Ao* aorta; *LA* left atrium; *PL* posterior leaflet; *AL* leaflet; *CR* chordae rupture; *MR* mitral regurgitation.

Figure 2.9.2 RT3DE. *Left*: full volume four-chamber view in systole. Posterior oblique view revealing CR and eversion of PL. *Center*: zoom 3D image from LV. Note how the P2 segment is moving away to the LA. *Right*: view from LA in systole, clearly demonstrating the ruptured segment (P2 moving to the LA). Note ruptured chordae inside the LA (*arrow*).

Figure 2.9.3 Color Doppler flow on RT3DE. *Left*: LV viewed through a hemisphere (*arrow*). Note the regurgitant orifice that is initiated between P2-A2 segments. *Right*: view of the LA through the regurgitant jet. Note the coanda-effect at the anterior wall of the LA (*arrows*).

Figure 2.9.4 Color Doppler flow on TEE 2DE. *Left*: note the highly eccentric shape of the regurgitant jet traveling from the PL to the inter-auricular septum. Due to its eccentricity, exact estimation of its origin is cumbersome with 2DE. *Right*: color Doppler on RT3DE enabling visualization and quantification of the regurgitant jet in three different spatial planes at each moment of the cardiac cycle. Note how the vena contracta diameter differs according to the spatial plane used due to its elliptical shape.

Case 2.10

Endomyocardial Fibrosis Secondary to a Hypereosinophilic Syndrome

A 57-year-old male complained of progressive dyspnea for almost a year and was referred for further evaluation of his heart failure. The patient had a long-standing history of parasitic infection and hypereosinophilia (>1,500/ml).

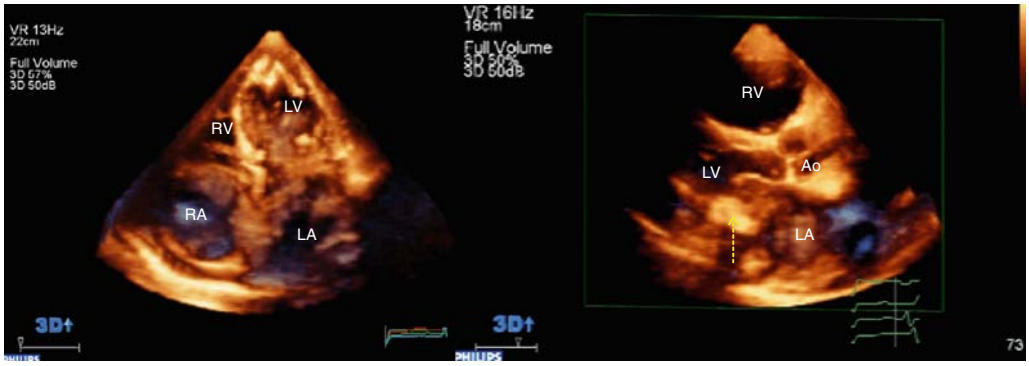

Fig. 2.10.1

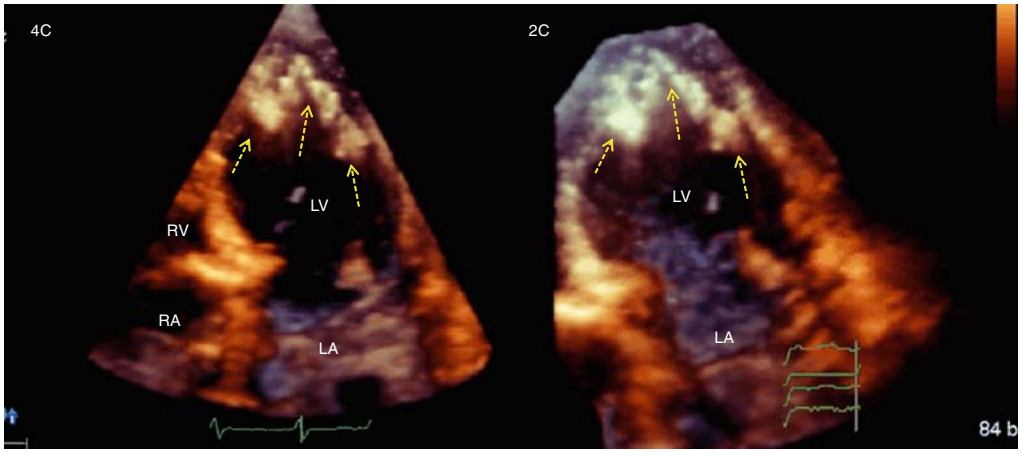

Fig. 2.10.2

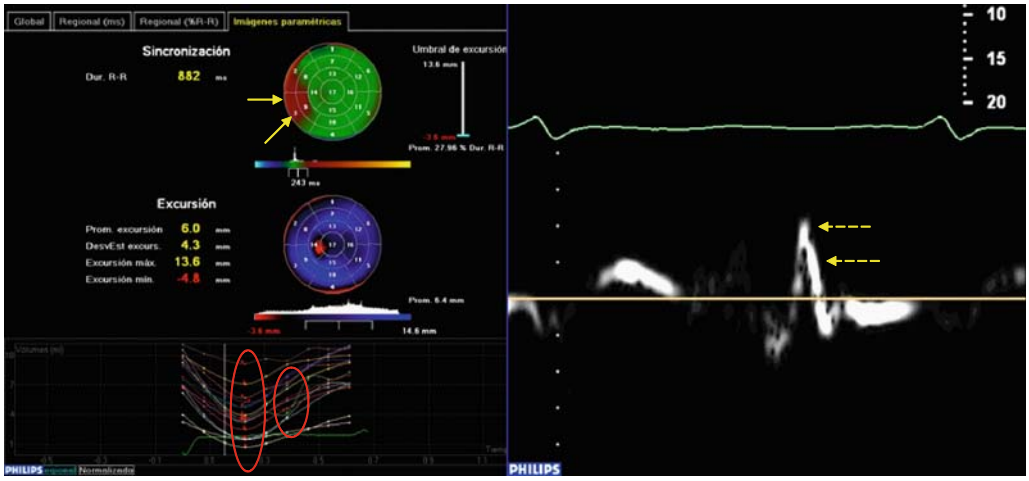

Fig. 2.10.3

Comments

Hypereosinophilic syndromes include endomyocardial fibrosis and Loeffler's endocarditis. These diseases are characterized by direct myocardial damage produced by eosinophilic cytotoxicity. Loeffler's endocarditis is part of an idiopathic hypereosinophilic syndrome. Endomyocardial fibrosis is endemic in African regions, India, and South America, and it is linked to parasitic infection. Endomyocardial fibrosis is usually due to the presence of dead parasites within the myocardium that provoke an inflammatory reaction and fibrosis. Myocardial microscopic evaluation shows intense fibrosis at the endocardium, especially at the apical regions of both right and left ventricles, obliterating both apexes. In addition, fibrosis may involve subvalvular tricuspid and mitral apparatus.

In the first phase of the disease, thrombus at the apexes may be visualized, followed by intense apical fibrosis and even calcification in some cases. These changes translate into alterations in ventricular filling, however, with still normal ventricular filling pressures and mild or absent clinical expression. During a later phase, fibrosis worsens resulting in a severe ventricular restrictive pattern and overt diastolic heart failure (left-side, right-side, or biventricular).

Echocardiography allows the direct diagnosis of the presence of small ventricles and dilated atriums. Color and tissue Doppler echo helps evaluate the patient's hemodynamic pattern and the degree of improvement with the instituted medical therapy.

Findings

Figure 2.10.1 Real-time 3D echocardiography (RT3DE). *Left*: four-chamber view showing severe left and right atrial dilation and left ventricular apical involvement. *Right*: longitudinal view, note mitral valve involvement by the disease. Posterior mitral leaflet is involved, showing intense calcification (*arrow*). The anterior mitral leaflet presents a dome-shaped opening.

Figure 2.10.2 RT3DE. Full 3D volume images obtained with angulation. Note a *round* calcification at the apex (*arrows*).

Figure 2.10.3 RT3DE. *Left*: 3D Echo Parametric Imaging derived from the left ventricular 3D volume. *Green* segments contract in a synchronous fashion. Note the presence of late contraction in *red* (*arrows*) that represent the proto-diastolic notch of the interventricular septum, characteristic of a restrictive physiology. *Right*: tissue Doppler imaging at the septum reveals a similar phenomenon (*dashed arrows*).

Case 2.11

Tako-Tsubo Syndrome

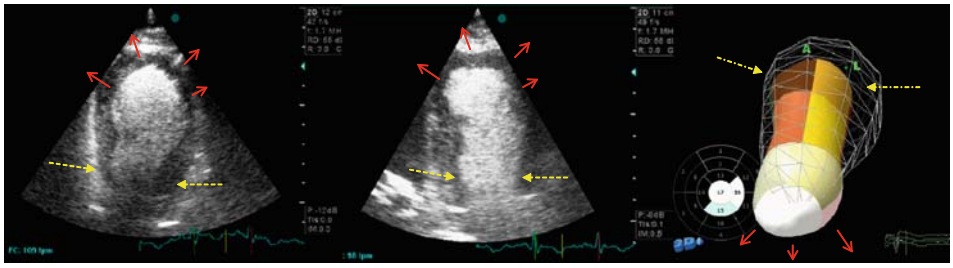

Fig. 2.11.1

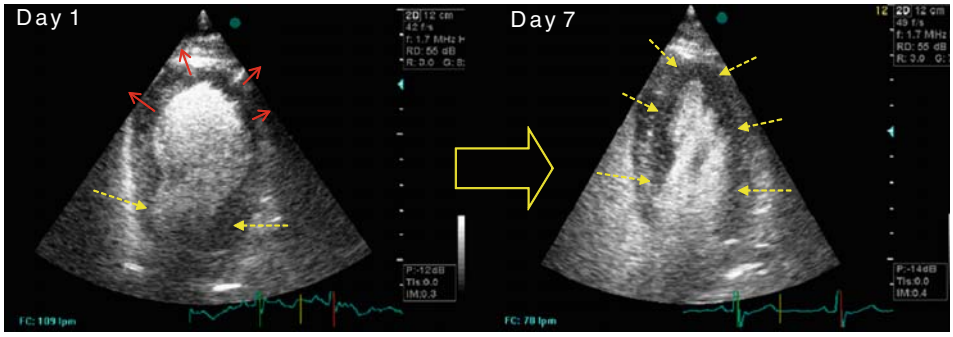

Fig. 2.11.2

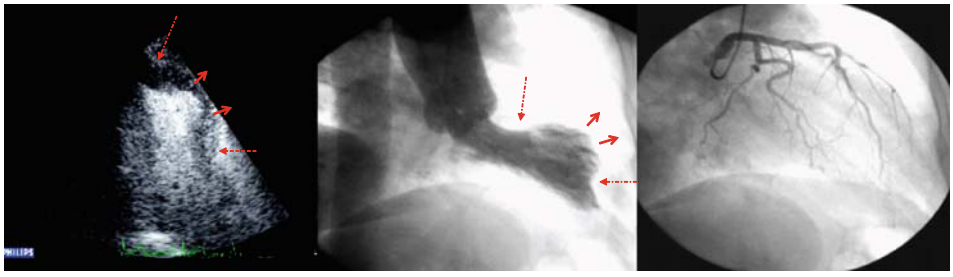

Fig. 2.11.3

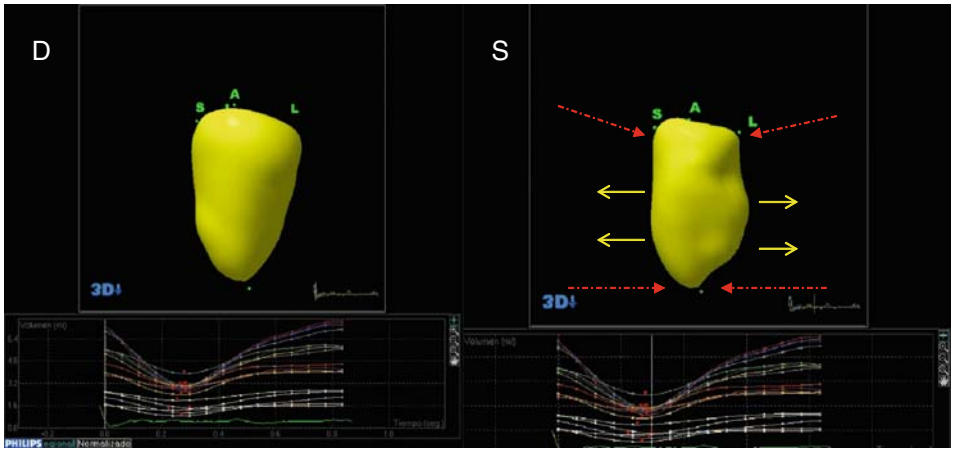

Fig. 2.11.4

We describe cases of two females, 55 and 67 years old, who both presented with prolonged precordial chest pain following deep emotional distress. The younger woman had a strong argument at her job and the older woman recently suffered the death of a beloved relative. Coronary angiogram ruled out obstructive epicardial stenosis in both cases.

Comments

The clinical presentation of Tako-Tsubo syndrome (TTS) is similar to that of acute coronary artery syndrome. TTS is far more frequent in females (i.e., 9:1 female/male ratio) and is usually preceded by emotional or physical stress in the absence of epicardial coronary lesions. It is characterized by transient dyskinesia/akinesia, frequently localized in the apex of the left ventricle (LV), although it can affect other areas of the LV such as the mid-ventricular area. In TTS it is common to find ECG abnormalities in the precordial leads and mild troponine elevation. Echocardiography is diagnostic, revealing pathognomonic LV segmental abnormalities in motility as previously described. In addition, echocardiography is essential for clinical follow-up, commonly observing normalization of ventricular segmental motility within 30 days.

Findings

Figure 2.10.1 Patient with transitory apical ballooning. *Left*: contrast echocardiography, four-chamber apical view showing mid-apical dyskinesia (*dashed arrows*). Center: same findings observed with two-chamber view. *Right*: real-time 3D echocardiogram (RT3DE), note the segmental abnormalities in 3D LV volume. Dyskinesia of the apical segments (*arrows*) and normal motility at the basal segments (*dashed arrows*).

Figure 2.10.2 *Left*: contrast echocardiography, four-chamber apical view on day 1 showing mid-apical diskenesia. *Right*: similar technique on day 7 showing improvement of apical segmental motility, while LV acquired normal shape.

Figure 2.10.3 Patient with transitory mid-ventricular dyskinesia. *Left*: contrast echocardiography, two-chamber apical view showing antero-medial dyskinesia. *Center*: contrast left ventriculogram during cardiac catheterization showing same echocardiographic findings. *Right*: coronary angiography with no significant left coronary lesions.

Figure 2.10.4 RT3DE, 3D LV volume. *Left*: (diastole) note normal morphology of the left ventricle during diastole. *Right*: (systole) note expansion of mid-ventricular LV (*arrows*) with normal motility at the basal and apical segments (*dashed arrows*).

Case 2.12

Rheumatic Mitral Stenosis

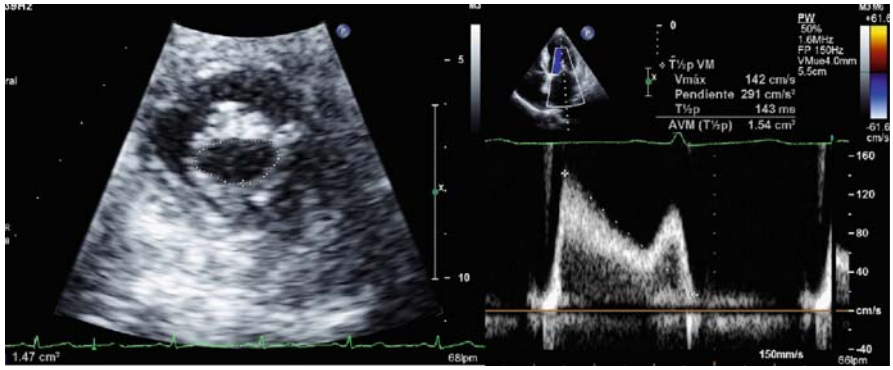

Fig. 2.12.1

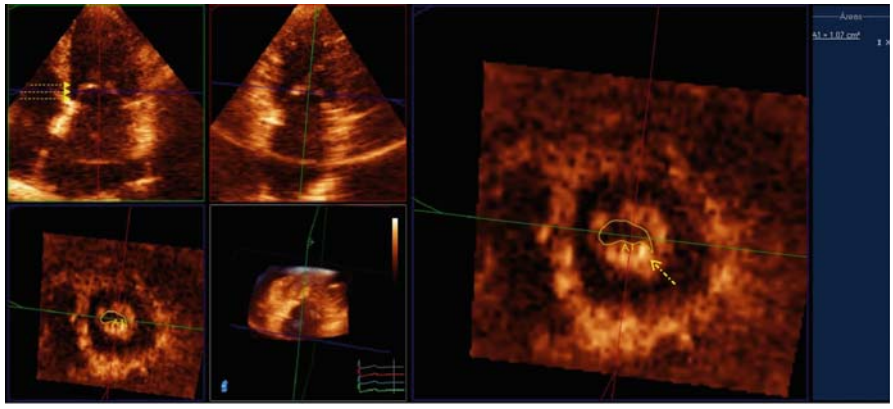

Fig. 2.12.2

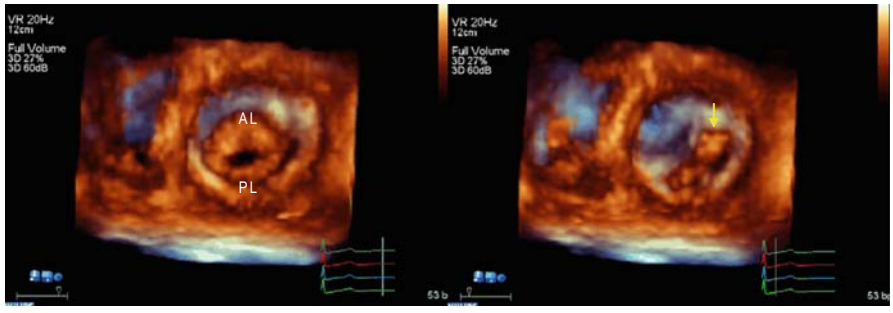

Fig. 2.12.3

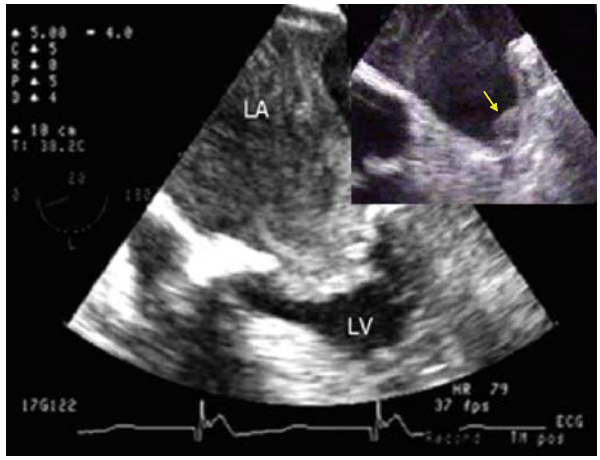

Fig. 2.12.4

A 68-year-old female with surgical commisurotomy 25 years ago was referred for an echocardiogram due to new-onset dyspnea on minimal exertion. An echocardiogram was performed to determine mitral area and select the appropriate therapeutic approach.

Comments

Despite reduction in rheumatic fever prevalence, rheumatic mitral stenosis (MS) remains a frequent cause of valvular disease in underdeveloped countries, representing 12% of all valvular cases. 2D and color Doppler echocardiography (2DE) precisely estimate the degree of stenosis and help select the best therapy for MS. Nevertheless, prior surgical procedures in the valve, uncontrolled atrial fibrillation, or concomitant presence of aortic insufficiency limit 2DE conventional assessment (i.e., planimetry, pressure half-time). In these cases, real-time 3D echocardiography (RT3DE) allows a more reliable quantification of MS than 2DE.

The ability to achieve multiple views of the mitral valve in different spatial planes allows adequate alignment with the valve and, hence, precise measurement of the valve area in the most stenotic region.

Furthermore, RT3DE offers detailed anatomical information of the valve and its apparatus, which is very useful to determine feasibility of percutaneous mitral valvuloplasty (PVM) and also guide the procedure. In patients who are candidates for PVM, transesophageal echocardiography (TEE) prior to the procedure is also needed to exclude thrombus in the atriums, which constitutes a contraindication for the percutaneous procedure.

Findings

Figure 2.12.1 2DE. *Left*: assessment of mitral valve area by planimetry. *Right*: Doppler tracing assessing pressure half-time. The area by both methods was 1.5 cm^2. Taking into account that the patient had prior open commisurotomy, the evaluation was further complemented with RT3DE.

Figure 2.12.2 RT3DE. *Left*: assessment of mitral area with multiplanar technique. RT3DE allows transversal view from annulus to the valvular border, until the minimum valvular orifice is encountered. The latter can be achieved without losing proper vertical axis alignment with the heart. *Right*: mitral area was 1.07 (significantly lower than with 2DE).

Figure 2.12.3 RT3DE assessed mitral valve structures. *Left*: (diastole) note considerable thickening of the valve with commissural fusion. *Right*: (systole) nodular calcification is observed at the antero-lateral commissure (*arrow*), which reduces PVM chances of success and increases risk of residual mitral insufficiency. *AL* anterior leaflet; *PL* posterior leaflet.

Figure 2.12.4 TEE: left atrium with severe spontaneous contrast. Zoomed image at the level of the left atrium appendage: note the presence of thrombus (*arrow*), which contraindicates PVM. *LA* left atrium; *LV* left ventricle.

Case 2.13
Atrial Septal Defect and Stroke

A 29-year-old female complaining of severe left hemicranial headache, diminished right-eye vision, nausea and vomiting presented to the emergency department. Physical examination revealed right superior quadrantanopsia. Head computed tomography showed occipital attenuation compatible with ischemia at the left posterior cerebral artery. Later on, a magnetic resonance imaging revealed cortical and subcortical edema of the left inferior occipital lobe compatible with a subacute ischemic lesion. ECG was normal. Transthoracic (TTE) and transesophageal echocardiogram (TEE) were done to seek a cardiovascular embolic source.

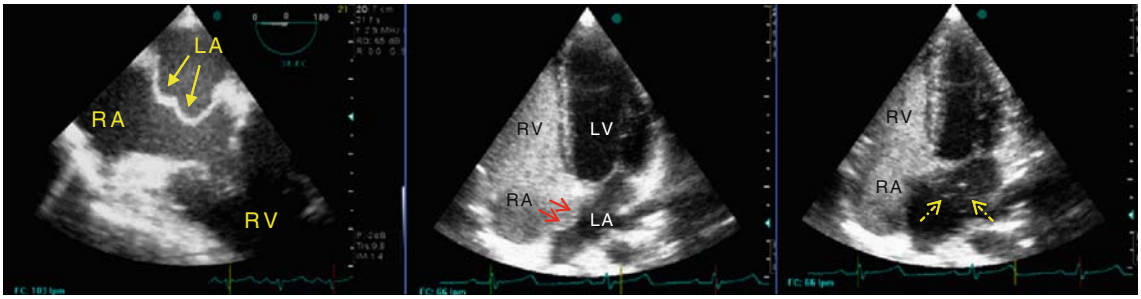

Fig. 2.13.1

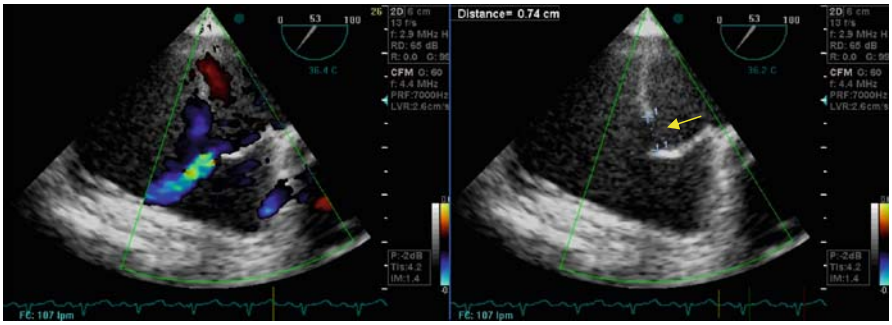

Fig. 2.13.2

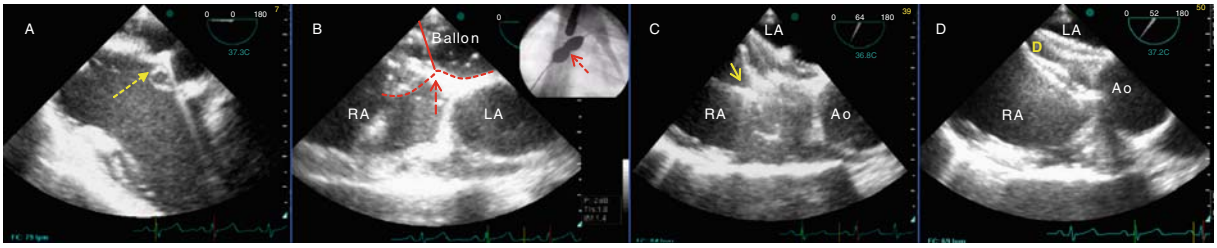

Fig. 2.13.3

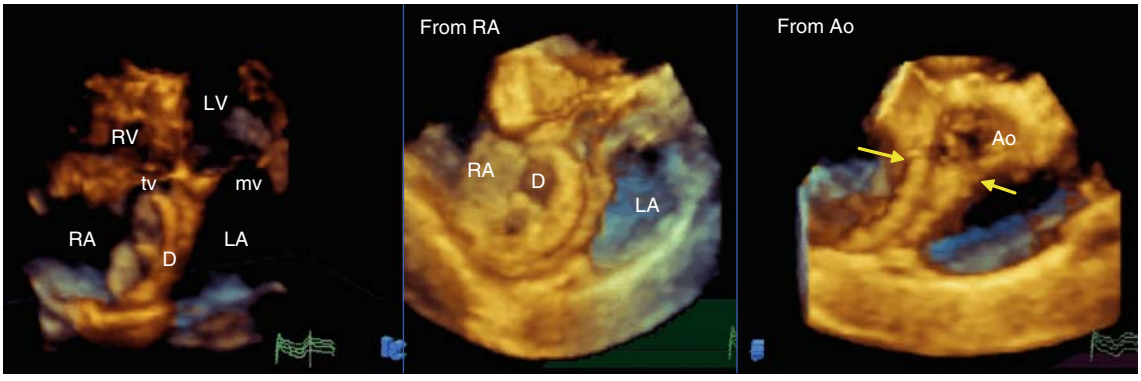

Fig. 2.13.4

Comments

Patent foramen ovale (PFO) and atrial septal aneurysm are shown to be at increased risk of ischemic stroke. In young patients with cryptogenic stroke, TTE and TEE are indicated while searching for an embolic source. TTE with agitated saline injection is very sensitive for the detection of PFO and constitutes the first diagnosis step. In this test, correct bubble visualization is performed with harmonic imaging during a Valsalva maneuver. TEE is essential and complementary to TTE, since its use provides detailed information of the atrial septum, which is particularly useful for diagnosis and selection of the best candidates for percutaneous closure. In addition, TEE provides useful guidance during the entire percutaneous procedure (i.e., crossing through the defect, measuring the orifice during balloon inflation, positioning and deployment of the device, assessment of immediate results, and exclusion of potential complications). Nowadays, TEE 3D offers superb anatomical evaluation and may possibly replace bidimensional evaluation in the near future.

Whenever atrial shunt is observed from right to left, the most frequent cause is an association of atrial septal aneurysm and PFO. In rare cases, right to left shunt can be observed in small punctiform atrial septal defects (ostium secundum). In atrial septal defects, the flow is predominantly left to right; thus, the occurrence of cerebrovascular accidents is very low. In the present case, we found a large atrial septal aneurysm with a small septal defect (7 mm) and predominant left to right flow. Nevertheless, in some cardiac beats, the atrial septum presented excursion to the left atrium (LA), detecting a minimal right to left shunt. Based on this observation, we proceeded with percutaneous closure with an Amplatzer device under TEE-guidance. The patient underwent a follow-up TEE 3D.

Findings

Figure 2.13.1 TEE. *Right*: conventional mid-esophageal 0° view. Note a large atrial septal aneurysm with a peculiar shape (bilobulated) and excursion to the right atrium (RA, *arrows*). *Center*: Transtoracic echocardiography, 4 chamber view with agitated saline. Note the excursion of the atrial septum to the LA during the relaxation phase, provoked by Valsalva maneuver (*red arrows*). *Left*: Same view by ETT. Note the bubbles passing to the LA (*dashed arrows*).

Figure 2.13.2 TEE. *Left*: color image, 53° view. Note shunt left to right compatible with atrial septal defect, ostium secundum type. *Right*: at the same view without color, note the 7 mm atrial septal defect (*arrow*).

Figure 2.13.3 TEE. Monitoring during percutaneous closure. (a) Threading of the guidewire through the septal defect (*arrow*). (b) Measurement of the defect during balloon inflation. The measurement is taken at the balloon notch (*arrow*). (c) Device with both discs spread out prior to deployment (*arrow*). (d) Assessment after device deployment showing adequate placement, adjacent to the aorta.

Figure 2.13.4 Follow-up evaluation with RT3DE. *Left*: full volume 3D (postprocessed), showing four chambers and their relationship with the device. *Center*: view from RA, showing its relationship with the tricuspid valve. *Right*: view from the aorta, showing the device (*arrow*) properly placed and its relationship with the aorta.

Case 2.14

Percutaneous Closure of Severe Paravalvular Leak

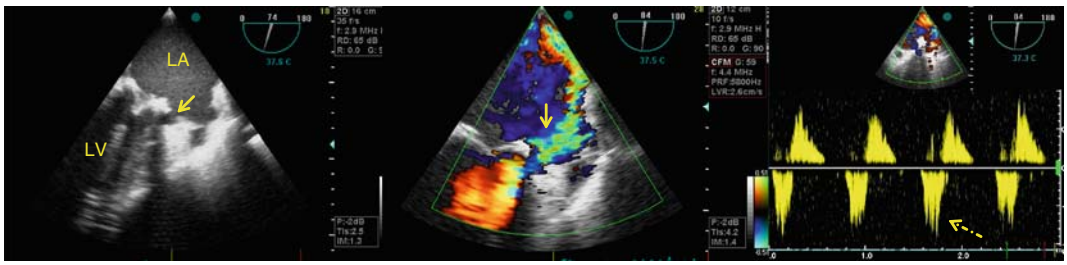

Fig. 2.14.1

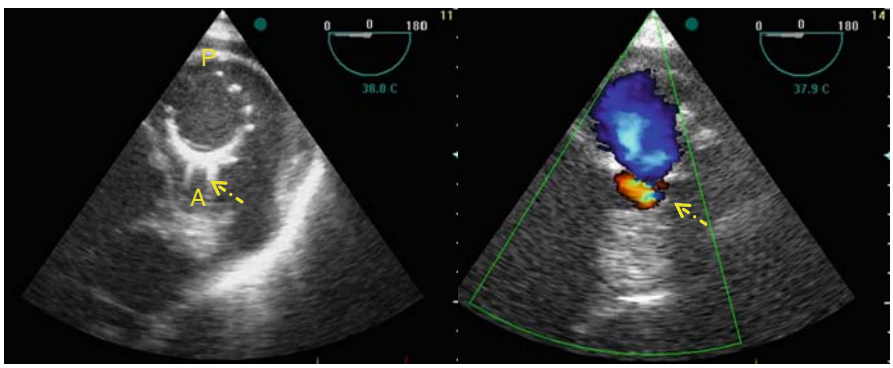

Fig. 2.14.2

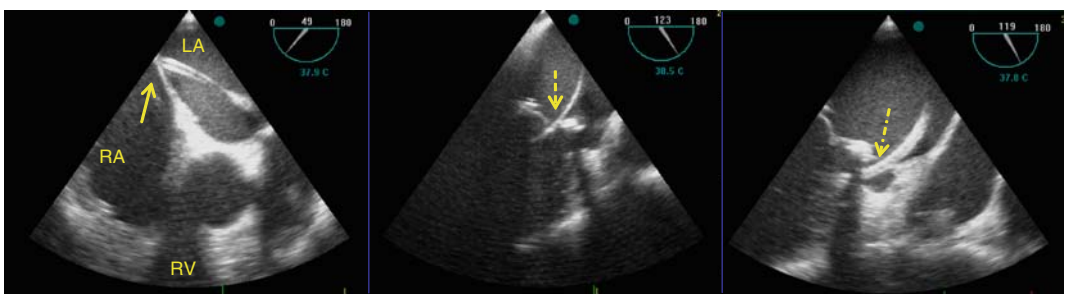

Fig. 2.14.3

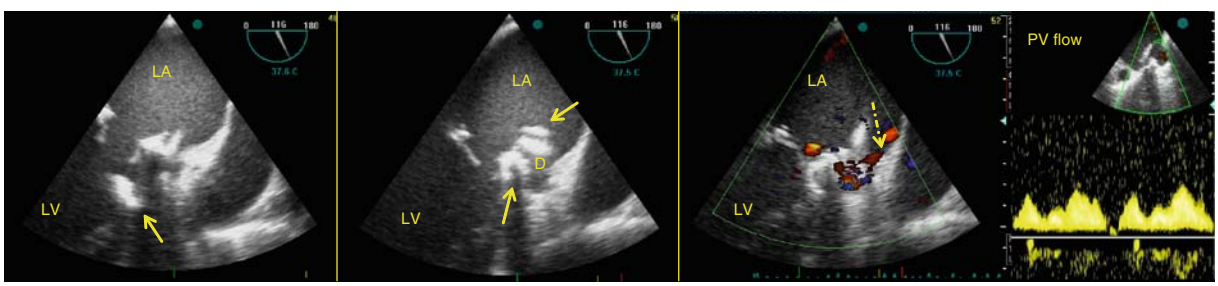

Fig. 2.14.4

An 83-year-old male, former smoker with prior surgical valve replacement (biological prosthesis) due to flail mitral valve 9 years ago, was admitted due to new-onset heart failure. Transesophageal echocardiography (TEE) revealed severe paravalvular leak (PVL) and the possibility of percutaneous closure was considered.

Comments

Reoperation for either replacement or repair of cardiac valve prosthesis is usually recommended in patients with significant PVL. However, in patients unsuitable for cardiac surgery, percutaneous closure of PVL may be considered. Percutaneous closure of PVL is usually performed under general anesthesia, with radiographic and TEE guidance. TEE provides a detailed analysis of the prosthetic dehiscence prior to the intervention, since it evaluates the degree of PVL, the shape and precise location of the dehiscence. During the procedure, TEE guides trans-septal puncture as well as the maneuver and placement of the closing device. Moreover, TEE allows adequate visualization during device deployment and assessment of immediate results (i.e., presence of residual leak). Finally, potential complications such as development of cardiac thrombi, prosthesis regurgitation, or blockade are excluded at the end of the procedure with TEE.

Findings

Figure 2.14.1 TEE. *Left*: conventional 74° view, note PVL on the anterior region (*arrow*), adjacent to the left atrium (LA) appendix. *Center*: color Doppler tracing at 84° view. Note the large periprosthetic regurgitant jet through the dehiscence (*arrow*). *Right*: pulsed Doppler image obtained at the level of the superior left pulmonary vein. Note systolic flow reversal secondary to severe mitral regurgitation (*arrow*). *RA* right atrium.

Figure 2.14.2 TEE. *Left*: conventional transgastric 0° view. *Right*: color Doppler image (systole) at the same level, note the regurgitant orifice at the anterior annular region (*arrow*). *A* anterior; *P* posterior.

Figure 2.14.3 Monitoring percutaneous closure of PVL by TEE (I). *Left*: Conventional, 49° view, showing a correctly localized trans-septal puncture (*arrow*). *Center*: incorrect threading of the guidewire through the valve leaflets (*arrow*). *Right*: correct passage of guidewire and introducer through the dehiscence orifice (*arrow*). *RV* right ventricle.

Figure 2.14.4 TEE. Monitoring percutaneous closure of PVL by TEE (II). *Left*: conventional 116° view, showing deployment of the first device disc at the ventricular side. *Center*: same view after deployment, showing correct placement with no interference in prosthetic valve function. *Right*: color Doppler at the same view, note minimal residual leak (*arrow*). Significant change in pulmonary vein flow pattern is observed with similar systolic and diastolic flow velocities. *LV* left ventricle; *D* device; *PV* pulmonary vein.

Case 2.15

Aortic Root Pseudoaneurysm Following Bentall Procedure

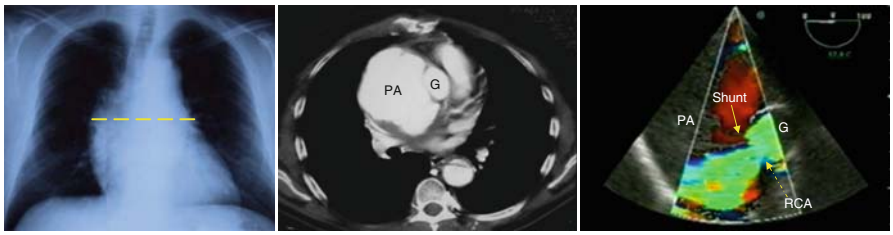

Fig. 2.15.1

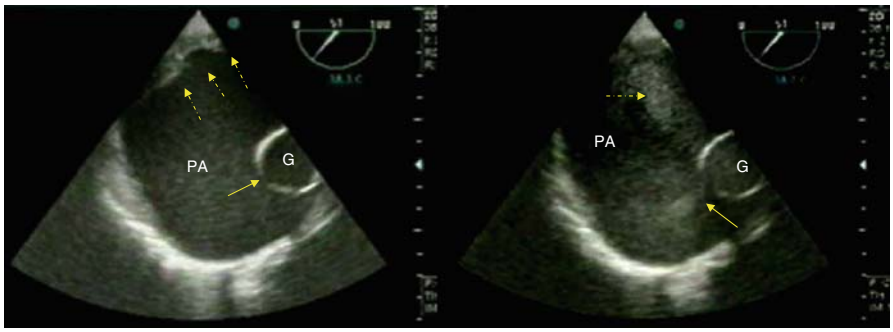

Fig. 2.15.2

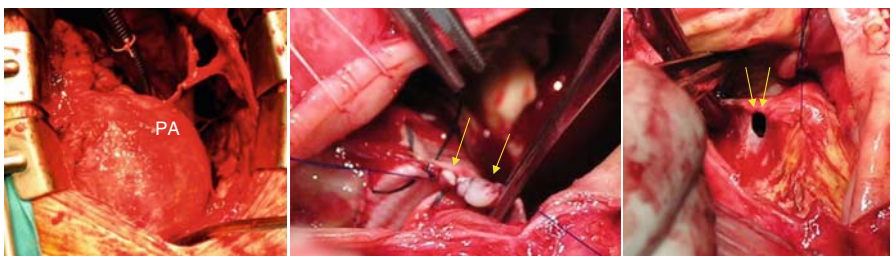

Fig. 2.15.3

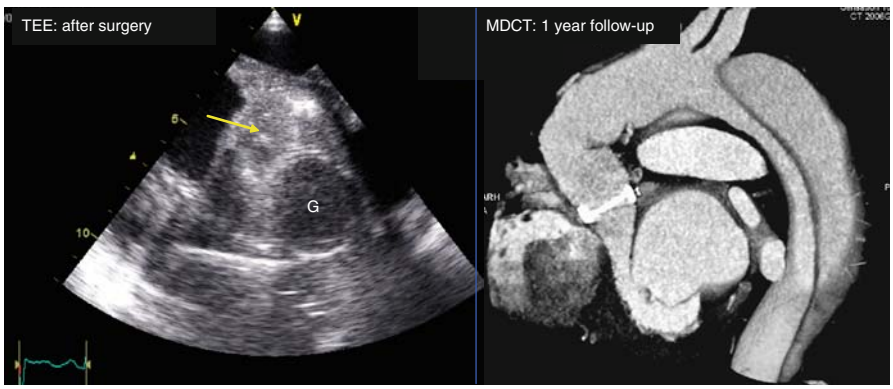

Fig. 2.15.4

We present a case of a 48-year-old hypertensive male with a family history of aortic dissection, and a prior history of aortic dissection type A (aorta 45 mm diameter), associated with moderate to severe aortic valve insufficiency (tricuspid valve) and obstruction of both right and left coronary ostium. The patient underwent a Bentall surgical procedure with concomitant myocardial revascularization (two vein grafts to left and right coronary arteries). Two months later, he returned to our clinic due to new onset of dyspnea and asthenia without signs of heart failure. Hemoglobin level was 9.6 mg/ml, hematocrit 25%. Transesophageal echocardiogram (TEE) and chest computed tomography were done.

Comments

The incidence of pseudoaneurysm formation unrelated to infection in patients who have undergone aortic root replacement (Bentall procedure) is at least 8–10%.

The communication point is more commonly situated at the suture of the right coronary ostium; however, communications may exist distal to the suture or fistulas to right atrium. Pseudoaneurysm formation can occur over variable lengths of time. Immediate postoperative and follow-up assessment by imaging techniques contributes to an early diagnosis and treatment of this complication. By providing substantial morphological and functional data, TEE remains superior to transthoracic (TTE) for the diagnosis of this complex complication. In addition, TEE conveys information regarding the communication points between the prosthetic tube and the pseudoaneurysm. Furthermore, TEE with contrast administration unmasked discrete communication points not diagnosed by other imaging techniques. The latter is vital prior to reoperation. Multislice computed tomography (MSCT) offers more detailed information with greater vision perspective. In many cases, multiple imaging techniques are necessary in order to perform a precise diagnosis and select the best surgical strategy.

Findings

Figure 2.15.1 *Left*: chest-X-ray during readmission to the hospital revealing a widened mediastinum. *Center*: Helicoidal CT demonstrating a cavity adjacent to the aorta with mural thrombus compatible with pseudoaneurysm (PA) formation. *Right*: color TEE at mid-esophageal 0° view. Note the jet from the graft to the pseudoaneurysm at the level of the proximal anastomosis of the vein grafted to right coronary artery (*arrow*).

Figure 2.15.2 TEE. *Left*: conventional image at mid-esophageal 0° view, note a large pseudoaneurysm with mural thrombus (*dashed arrows*). Note complete tear of the proximal anastomosis to right coronary artery (*arrow*). *Right*: contrast image at the same view, revealing the presence of two jets. One jet communicates the graft to pulmonary artery through the tear of the proximal anastomosis of the vein graft (*arrow*), while a second jet communicates the graft to the right atrium (*dashed arrow*). The start point of the jet is not visualized at the origin in this image.

Figure 2.15.3 Images during surgery. *Left*: external view of the pseudoaneurysm. *Center*: Suture of the vein graft tear to right coronary artery (*arrows*). *Left*: Communication orifice to right atrium (*arrow*).

Figure 2.15.4 *Left*: postoperative TEE at day 1. Note a hematoma adjacent to the tube without internal flow (*arrow*). *Right*: MSCT. Follow-up after 1 year, showing resolution of pseudoaneurysm.

Further Reading

Books

Textbook of Clinical Echocardiography, 3rd ed. Catherine M. Otto (2004) Saunders, Philadelphia

Feigenbaum's Echocardiography. Harvey Feigenbaum, William Armstrong (2004) Lippincott Williams & Wilkins, Philadelphia

The Echo Manual. Jae K. Oh, James B. Seward (2006) Lippincott Williams & Wilkins, Philadelphia

Atlas of Transesophageal Echocardiography. Navin C. Nanda, Michael J. Domanski (2006) Lippincott Williams & Wilkins, Philadelphia

Doppler Myocardial Imaging. A Textbook. George.R Sutherland, Liv Hatle, Piet Claus Jan D' hooge, Bart Bijnens (2006) BSWK, Belgium

Atlas of Intraoperative Transesophageal Echocardiography: Surgical and Radiologic Correlations, Textbook with DVD. Donald Oxorn; Catherine M. Otto (2007) Saunders, Philadelphia

3-D Echocardiography, An Issue of Cardiology Clinics. Edward A. Gill, N. Nanda (2007) Saunders, Philadelphia

López de Sá E, López-Sendón JL, Rubio R. Infarto agudo de miocardio: clínica, evolución y complicaciones. In: Delcán JL (ed) Cardiopatía isquémica. ENE ediciones, Madrid, 1999; 583–584

Rotura Cardiaca Isquémica. Text book. Figueras J, Soler Soler J (2001) Editorial, Doyma

Sbar S, Harrison EE. Chronic tricuspid insufficiency due to trauma. In: Hurst JW (ed) The Heart: Update III. McGraw-Hill, New York, 1980; 43–51

Interactive CD of Echocardiography

Clinical Echocardiography. Arturo Evangelista, Herminio Garcia del Castillo. Co-authors: Teresa Gonzalez Alujas, Gustavo Avegliano, Zamira Bosch. The Academy of Medical Ultrasound. Supported by GE Healthcare, 2004

Web-Links

http://www.wiley.com/bw/journal.asp?ref=0742–2822
http://www.med.yale.edu/intmed/cardio/echo_atlas/contents/index.html
http://asecho.org/
http://journals.elsevierhealth.com/periodicals/ymje
http://www.interscience.wiley.com/jpages/0742–2822
http://www.sciencedirect.com/science/journal/08947317
http://www.escardio.org

Articles

Abad C. Tumores cardiacos (II). Tumores primitivos malignos. Tumores metastásicos. Tumor carcinoide. Rev Esp Cardiol 1998; 51:103–114

Abinder E, Sharif D, Shefer A et al Novel insights into the natural history of apical hypetrophic cardiomyopathy during long-term follow-up. IMAJ 2002; 4:166–169

Acebo E, Val-Bernal JF, Gómez Román JJ. Thrombomodulin, calretinin and c-kit (CD117) expression in cardiac myxoma. Histol Histopathol 2001; 16:1031–1036

Ako J. Apical and midventricular transient left ventricular dysfunction syndrome (tako-tsubo cardiomyopathy). Chest 2008; 133(4):1052; author reply 1053

Alcalai R, Seidman J, Seidman C et al Genetic basis of hypertrophic cardiomyopathy: from bench to the clinics J Cardiovasc Electrophysiol 2008; 19:104–110

Almendro-Delia M, Hidalgo-Urbano R. Transient midventricular dyskinesia: tako-tsubo cardiomyopathy. The story continues. Rev Esp Cardiol 2008; 61(11):1223–1224

Aoyagi S, Kosuga K, Akashi H, Oryoji A, Oishi K. Aortic root replacement with a composite graft: results of 69 operations in 66 patients. Ann Thorac Surg 1994; 58:1469–1475

Armstrong WF, Bach DS, Carey LM, Froehlich J, Lowell M, Kazerooni EA. Clinical and echocardiographic findings in patients with suspected acute aortic dissection. Am Heart J 1998; 136:1051–1060

Avegliano G, Evangelista A, Elorz C, González-Alujas T, García del Castillo H, Soler-Soler J. Acute peripheral arterial ischemia and suspected aortic dissection: usefulness of transesophageal echocardiography in differential diagnosis with aortic thrombosis. Am J Cardiol 2002; 90(6):674–677

Belghiti H, Aouad A, Arharbi M. Suspected left-ventricular noncompaction on two- and three-dimensional echocardiography: is it always clear? Arch Card Dis 2008; 101:373–374

Berensztein CS, Piñeiro D, Marcotegui M, Brunoldi R, Blanco MV, Lerman J. Usefulness of echocardiography and Doppler echocardiography in endomyocardial fibrosis. J Am Soc Echocardiogr 2000; 13(5):385–392

Bicudo LS, Tsutsui JM, Shiozaki A et al Value of real time three-dimensional echocardiography in patients with hypertrophic cardiomyopathy: comparison with two-dimensional echocardiography and magnetic resonance imaging. Echocardiography 2008; 25:717–726

Biorck G, Mogensen L, Nyquist O, Orinius E, Sjogren A. Studies of myocardial rupture with tamponade in acute myocardial infarction: clinical features. Chest 1972; 61:4–6

Blockmans D, Bley T, Schmidt W. Imaging for large-vessel vasculitis. Curr Opin Rheumatol 2009; 21(1):19–28

Both M, Ahmadi-Simab K, Reuter M, Dourvos O, Fritzer E, Ullrich S, Gross WL, Heller M, Bähre M. MRI and FDG-PET in the assessment of inflammatory aortic arch syndrome in complicated courses of giant cell arteritis. Ann Rheum Dis 2008; 67(7):1030–1033

Botto F, Trivi M, Padilla LT. Transient left midventricular ballooning without apical involvement. Int J Cardiol 2008; 127(3):e158–e159

Breithardt OA, Becker M, Kälsch T, Haghi D. Follow-up in Takotsubo cardiomyopathy by real-time three-dimensional echocardiography. Heart 2008; 94(2):210

Brian C, Weiford MD, Vijay D, Subbarao MD, Kevin M, Mulhern MD. Noncompaction of the ventricular myocardium. Circulation 2004; 109:2965–2971

Bizzarri F, Mattia C, Ricci M, Coluzzi F, Petrozza V, Frati G, Pugliese G, Muzzi L. Cardiogenic shock as a complication of acute mitral valve regurgitation following posteromedial papillary muscle infarction in the absence of coronary artery disease. J Cardiothorac Surg 2008; 3:61

Cellarier G, Cuguillière A, Gisserot O, Laurent P, Bouchiat C, Bonal J, Talard P, Dussarat GV. Acute complication of a composite graft replacement of the aortic root. J Mal Vasc 1999; 24(5):381–383

Chan KL. Usefulness of transesophageal echocardiography in the diagnosis of conditions mimicking aortic dissection. Am Heart J 1991; 122:495–504

Chin TK, Perloff JK, Williams RG et al Isolated noncompaction of left ventricular myocardium: a study of eight cases. Circulation 1990; 82:507–513

Chirillo F et al Usefulness of transthoracic and transoesophageal echocardiography in recognition and management of cardiovascular injuries after blunt chest trauma. Heart 1996; 75(3):301–306

Costabel JP, Avegliano G et al Miocardiopatía hipertrófica apical que simula um síndrome coronario agudo. Utilidad de la ecocardiografía tridimensional. Rev Argent Cardiol 2008; 76:488–490 (spanish text)

Daniel WG, Nellessen U, Schröder E, Nonnast-Daniel B, Bednarski P, Nikutta P, Lichtlen PR. Left atrial spontaneous echo contrast in mitral valve disease: an indicator for an increased thromboembolic risk. J Am Coll Cardiol 1988; 11(6):1204–1211

DeBakey ME, McCollum CH, Crawford ES. Dissection and dissecting aneurysms of the aorta: twenty-year follow-up of five hundred twenty-seven patients treated surgically. Surgery 1982; 92:1118–1134

Delgado Ramis L, Montiel J, Arís A, Caralps JM. Rotura traumática de la válvula tricúspide: presentación de tres casos. Rev Esp Cardiol 2000; 53:874–877

Eliot RS, Baroldi G, Leone A. Necropsy studies in myocardial infarction with minimal or no coronary luminal reduction due to atherosclerosis. Circulation 1974; 49(6):1127–1131

Erbel R, Börner N, Bruñiré J et al Detection of aortic dissection by transoesophageal echocardiography. Br Heart J 1987; 58: 45–51

Ericsson M, Sonnenberg B, Woo A et al Long-term outcome in patients with apical hypertrophic cardiomyopathy. J Am Coll Cardiol 2002; 39(4):638–645

Evangelista A. Puesta al día en el diagnóstico y tratamiento del sindróme aórtico agudo. Rev Esp Cardiol 2007; 60(4):428–439

Evangelista A, González Alujas T, Garcia del Castillo H et al Ecocardiografía transesofágica en el diagnóstico de la disección aórtica. Rev Esp Cardiol 1993; 46:805–809

Fabricius AM, Walther T, Falk V, Mohr FW. Three-dimensional echocardiography for planning of mitral valve surgery: current applicability?Ann Thorac Surg 2004; 78(2):575–578

Figueras J, Alcalde O, Barrabés JA, Serra V, Alguersuari J, Cortadellas J, Lidón RM. Changes in hospital mortality rates in 425 patients with acute ST-elevation myocardial infarction and cardiac rupture over a 30-year period. Circulation 2008; 118(25):2783–2789

Figueras J, Cortadellas J, Calvo F, Soler-Soler J. Relevance of delayed hospital admission on development of cardiac rupture during acute myocardial infarction: study in 225 patients with free wall, septal or papillary muscle rupture. J Am Coll Cardiol 1998; 32:135–139

Frans E, Nanda N, Patel V et al Live three dimensional transthoracic contrast echocardiographic assessment of apical cardiomyopathy. Ecocardiography 2005; 22(8)686–689

Gayet C, Pierre B, Delahaye J, Champsaur G, Andre-Fouet X, Rueff P. Traumatic tricuspid insufficiency, an underdiagnosed disease. Chest 1987; 92:429–432

Gopalamurugan AB, Kapetanakis S, Monaghan M. Left ventricular non-compaction diagnosed by real time three dimensional echocardiography. Heart 2005; 10:1274

Gutiérrez-Chico JL, Zamorano Gómez JL, Rodrigo-López JL, Mataix L, Pérez de Isla L, Almería-Valera C, Aubele A, Macaya-Miguel C. Accuracy of real-time 3-dimensional echocardiography in the assessment of mitral prolapse. Is transesophageal echocardiography still mandatory? Am Heart J 2008; 155(4): 694–698

Haddad M, Veinot JP, Masters RG, Hendry PJ. Essential thrombocytosis causing a massive myocardial infarction. Cardiovasc Pathol 2003; 12(4):216–218

Hagan PG, Nienaber CA, Isselbacher EM, Bruckman D, Karavite DJ, Russman PL, Evangelista A. The international registry of acute aortic dissection (IRAD). New insights into an old disease. JAMA 2000; 283:897–903

Hirata K, Pulerwitz T, Sciacca R, Otsuka R, Oe Y, Fujikura K, Oe H, Hozumi T, Yoshiyama M, Yoshikawa J, Di Tullio M, Homma S. Clinical utility of new real time three-dimensional transthoracic echocardiography in assessment of mitral valve prolapse. Echocardiography 2008; 25(5):482–488

Hozumi T, Yoshikawa J, Yoshida K, Akasaka T, Takagi T, Yamamuro A. Assessment of flail mitral leaflets by dynamic three-dimensional echocardiographic imaging. Am J Cardiol 1997; 79(2): 223–225

Hutt MS. Epidemiology aspects of endomyocardial fibrosis. Postgrad Med J 1983; 59(689):142–146

Illarroel MT et al Traumatic tricuspid insufficiency. Rev Esp Cardiol 1989; 42(2):145–147

Jenni R, Oechslin E, Schneider J, Attenhofer Jost C, Kaufmann PA. Echocardiographic and pathoanatomical characteristics of isolated left ventricular non-compaction: a step towards classification as a distinct cardiomyopathy. Heart 2001; 86(6): 666–671

Jenni R, Oechslin EN, van der Loo B. Isolated ventricular noncompaction of the myocardium in adults. Heart 2007; 93(1): 11–15

Kitaoka H, Doi Y, Casey S, Hitomi N et al Comparison of prevalence of apical hypertrophic cardiomyopathy in Japan and the United States. Am J Cardiol 2003; 92(10):1183–1186

Koo BK, Choi D, Ha J et al Isolated noncompaction of the ventricular myocardium: contrast echocardiographic findings and review of the literature. Echocardiography 2002; 19:153–156

Kouchoukos NT, Wareing TH, Murphy SF, Perrillo JB. Sixteen-year experience with aortic root replacement. Results of 172 operations. Ann Surg 1991; 214:308–320

Kuppahally SS, Paloma A, Craig Miller D, Schnittger I, Liang D. Multiplanar visualization in 3D transthoracic echocardiography for precise delineation of mitral valve pathology. Echocardiography 2008; 25(1):84–87

Kühl HP, Hoffmann R, Merx MW, Franke A, Klötzsch C, Lepper W, Reineke T, Noth J, Hanrath P. Transthoracic echocardiography using second harmonic imaging: diagnostic alternative to transesophageal echocardiography for the detection of atrial right to left shunt in patients with cerebral embolic events. J Am Coll Cardiol 1999; 34(6):1823–1830

Laraudogoitia E, Evangelista A, Garci'a del Castillo H, Lekuona I, Palomar S, González Alujas T, Salcedo A. Thombus of the thoracic aorta as a source of peripheral embolism diagnosed by transesophageal echocardiography. Rev EspCardiol 1997; 50:62–64

Laperche T, Laurian C, Roudaut R, Steg G. Mobile thromboses of the aortic arch without aortic debris. A transesophageal echocardiographic finding associated with unexplained arterial embolism. Circulation 1997; 96:288–294

López-Sendón J, González A, López de Sá E, Coma-Canella I, Roldán I, Domínguez F et al Diagnosis of subacute ventricular

wall rupture after acute myocardial infarction: sensitivity and specificity of clinical, hemodynamic and echocardiographic criteria. J Am Coll Cardiol 1992; 19:1145–1153
Mattioli AV, Aquilina M, Oldani A, Longhini C, Mattioli G. Atrial septal aneurysm as a cardioembolic source in adult patients with stroke and normal carotid arteries. A multicentre study. Eur Heart J 2001; 22(3):261–268
Messika-Zeitoun D, Brochet E, Holmin C, Rosenbaum D, Cormier B, Serfaty JM, Iung B, Vahanian A. Three-dimensional evaluation of the mitral valve area and commissural opening before and after percutaneous mitral commissurotomy in patients with mitral stenosis. Eur Heart J 2007; 28(1):72–79
Miller DC, Mitchell RS, Oyer PE, Stinson EB, Jamieson SW, Shumway NE. Independent determinants of operative mortality for patients with aortic dissections. Circulation 1984; 70(suppl I):I-153–I-164
Moon J, Fisher N, McKenna W et al Detection of apical hypertrophic cardiomyopathy by cardiovascular magnetic resonance in patients with non-diagnostic echocardiography. Heart 2007; 90(6)645–649
Moukarbel G, Alam S, Abchee A. Contrast-enhanced echocardiography for the diagnosis of apical hypertrophic cardiomyopathy. Echocardiography 2005; 22:831–833
Müller S, Müller L, Laufer G, Alber H, Dichtl W, Frick M, Pachinger O, Bartel T. Comparison of three-dimensional imaging to transesophageal echocardiography for preoperative evaluation in mitral valve prolapse. Am J Cardiol 2006; 98(2): 243–248
Naja I, Barriuso C, Ninot S, Martínez C, Oller G, Nolla M et al Rotura traumática de la válvula tricúspide. Tratamiento quirúrgico conservador. Rev Esp Cardiol 1992; 45:64–66
Oechslin E, Jenni R. Isolated left ventricular non-compaction: increasing recognition of this distinct, yet 'unclassified' cardiomyopathy. Eur J Echocardiogr 2002; 3(4):250–251
Omeroglu SN, Mansuroglu D, Goksedef D, Cevat Y. Ultrafast computed tomography in management of post-bentall aortic root pseudoaneurysm repair. Tex Heart Inst J 2005; 32(1): 91–94
Oliva PO, Hammill SC, Edwards WE. Cardiac rupture, a clinically predictable complication of acute myo-cardial infarction: report of 70 cases with clinicopathologic correlations. J Am Coll Cardiol 1993; 22:720–726
Orihashi K, Sueda T, Okada K, Imai K. Perioperative diagnosis of mesenteric ischemia in acute aortic dissection by transesophageal echocardiography. Eur J Cardiothorac Surg 2005; 28(6): 871–876
Pacifico L, Spodick D. ILEAD-ischemia of the lower extremities due to aortic dissection: the isolated presentation. Clin Cardiol 1999; 22:353–356
Pappas PJ, Cernainau AC, Baldino WA, Cilley JH Jr, Del Rossi AJ. Ventricular free wall rupture after myocardial infarction: treatment and outcome. Chest 1991; 99:892–895
Patel AK, D'Arbela PG, Somers K. Endomyocardial fibrosis and eosinophilia. Br Heart J 1977; 39(3):238–241
Patel KC, Pennell D, Leyva-Leon F. Left ventricular trabecular non-compaction. Heart 2004; 90(9):1076
Perez de Isla L, Casanova C, Almería C, Rodrigo JL, Cordeiro P, Mataix L, Aubele AL, Lang R, Zamorano JL. Which method should be the reference method to evaluate the severity of rheumatic mitral stenosis? Gorlin's method versus 3D-echo. Eur J Echocardiogr 2007; 8(6):470–473
Pepi M, Tamborini G, Maltagliati A, Galli CA, Sisillo E, Salvi L, Naliato M, Porqueddu M, Parolari A, Zanobini M, Alamanni F. Head-to-head comparison of two- and three-dimensional transthoracic and transesophageal echocardiography in the localization of mitral valve prolapse. J Am Coll Cardiol 2006; 48(12):2524–2530
Petersen SE, Selvanayagam JB, Wiesmann F, Robson MD, Francis JM, Anderson RH, Watkins H, Neubauer S. Left ventricular non-compaction: insights from cardiovascular magnetic resonance imaging. J Am Coll Cardiol. 2005 5;46(1):101–5
Pinar Sopena J, Candell Riera J, San José Laporte A, Bosch Gil J, García del Castillo H, Vilardell Tarres M, Soler Soler J. Echocardiographic manifestations in patients with hypereosinophilia. Rev Esp Cardiol 1990; 43(7):450–456 (Spanish)
Pothineni KR, Duncan K, Yelamanchili P, Nanda NC et al Live/real time three-dimensional transthoracic echocardiographic assessment of tricuspid valve pathology: incremental value over the two-dimensional technique. Echocardiography 2007; 24(5): 541–552
Prichard RW. Tumors of the heart: review of the subject and report of one hundred and fifty cases. Arch Patol 1951; 51: 98–128
Ramphal PS, Spencer HW, Mitchell DI. Myxoma of right femoralvein origin presenting as right atrial mass with syncope. J Thorac Cardiovasc Surg 1998; 116:655–656
Reddy VK, Nanda S, Bandarupalli N, Pothineni KR, Nanda NC. Traumatic tricuspid papillary muscle and chordae rupture: emerging role of three-dimensional echocardiography. Echocardiography 2008; 25(6):653–657
Reynen K. Cardiac myxomas. N Engl J Med 1995; 333: 1610–1617
Reyen K. Frequency of primary tumors of the heart. Am J Cardiol 1996; 77:107
Roberts WC. Primary and secondary neoplasms of the heart. Am J Cardiol 1997; 80:671–682
Russo A, Suri RM, Grigioni F, Roger VL, Oh JK, Mahoney DW, Schaff HV, Enriquez-Sarano M. Clinical outcome after surgical correction of mitral regurgitation due to papillary muscle rupture. Circulation 2008; 118(15):1528–1534
Saffitz JE, Phillips ER, Temesy-Armos PN, Roberts WC. Thrombocytosis and fatal coronary heart disease. Am J Cardiol 1983; 52(5):651–652
Seelos KC, Funari M, Higgins CB. Detection of aortic arch thrombus using MR imaging. J Comput Assist Tomogr 1991; 15:244–247
Sharma R, Mann J, Drummond L, Livesey SA, Simpson IA. The evaluation of real-time 3-dimensional transthoracic echocardiography for the preoperative functional assessment of patients with mitral valve prolapse: a comparison with 2-dimensional transesophageal echocardiography. J Am Soc Echocardiogr 2007; 20(8):934–940
Soyer H, Laudinat JM, Lemaitre C, Pommier JL, Delepine G, Poncet A, Baehrel B, Bajolet A. Recurrent mobile thrombus of the ascending aorta diagnosed by transesophageal echocardiography. Arch Mal Coeur 1993; 86:1769–1771
Spry CJ, Take M, Tai PC. Eosinophilic disorders affecting the myocardium and endocardium: a review. Heart Vessels Suppl 1985; 1:240–242
Suzuki T, Metha R, Ince H, Nagai R, Sakomura Y, Weber F. Clinical profiles and outcomes of acute type B aortic dissection in the current era: lessons from the International Registry of Aortic Dissection (IRAD). Circulation 2003; 108(suppl II): II-312–II-317
Szczytowski JM, Mixon TA, Santos RA, Lawrence ME. Images in cardiovascular medicine. A 54-year-old woman with chest

pain, dyspnea, and inferior injury on electrocardiography. Circulation 2006; 113(23):e852

Terracciano LM, Mhawech P, Suess K, D'Armiento M, Lehmann FS, Jundt G et al Calretinin as a marker for cardiac myxoma. Diagnostic and histogenetic considerations. Am J Clin Pathol 2000; 114:754–759

Van Son J, Danielson G, Schaff H, Miller F. Traumatic tricuspid valve insufficiency. J Thorac Cardiovasc Surg 1994; 108: 893–898

Varnava AM. Isolated left ventricular non-compaction: a distinct cardiomyopathy? Heart 2001; 86(6):599–600

Virmani R, Popovsky MA, Roberts WC. Thrombocytosis, coronary thrombosis and acute myocardial infarction. Am J Med 1979; 67(3):498–506

Vitebskiy S, Fox K, Hoit BD. Routine transesophageal echocardiography for the evaluation of cerebral emboli in elderly patients. Echocardiography 2005; 22(9):770–774

Wells KE, Alexander JJ, Piotrowski JJ, Finkelhor RS. Massive aortic thrombus det ected by transesophageal echocardiography as a cause of peripheral emboli in young patients. Am Heart J 1996; 132:882–883

Young JR, Kramer J, Humphries AW. The ischemic leg: a clue to dissecting aneurysm. Cardiovasc Clin 1975; 7:201–205

Zamorano J, Cordeiro P, Sugeng L, Perez de Isla L, Weinert L, Macaya C, Rodríguez E, Lang RM. Real-time three-dimensional echocardiography for rheumatic mitral valve stenosis evaluation: an accurate and novel approach. J Am Coll Cardiol 2004; 43(11):2091–2096

Zamorano J, Perez de Isla L, Sugeng L, Cordeiro P, Rodrigo JL, Almeria C, Weinert L, Feldman T, Macaya C, Lang RM, Hernandez Antolin R. Non-invasive assessment of mitral valve area during percutaneous balloon mitral valvuloplasty: role of real-time 3D echocardiography. Eur Heart J 2004; 25(23):2086–2091